Available online at www.sciencedirect.com

ScienceDirect

Geochimica et Cosmochimica Acta 120 (2013) 220–238

Geochimica et Cosmochimica Acta

www.elsevier.com/locate/gca

Combining sedimentological, trace metal (Mn, Mo) and molecular evidence for reconstructing past water-column redox conditions: The example of meromictic Lake Cadagno (Swiss Alps)

Stefanie B. Wirth [a,*], Adrian Gilli [a], Helge Niemann [b], Tais W. Dahl [c], Damiana Ravasi [d], Nadja Sax [b], Yvonne Hamann [a], Raffaele Peduzzi [d], Sandro Peduzzi [d,e], Mauro Tonolla [d,e,f], Moritz F. Lehmann [b], Flavio S. Anselmetti [g,1]

[a] *Geological Institute, ETH Zurich, Zurich, Switzerland*
[b] *Department of Environmental Sciences, University of Basel, Basel, Switzerland*
[c] *Institute of Biology and NordCEE, University of Southern Denmark, Odense, Denmark*
[d] *Alpine Biology Centre Foundation, Piora, Switzerland*
[e] *Institute of Microbiology, Canton Ticino, Bellinzona, Switzerland*
[f] *Microbiology Unit, Department of Botany and Plant Biology, University of Geneva, Geneva, Switzerland*
[g] *Eawag, Swiss Federal Institute of Aquatic Science and Technology, Dübendorf, Switzerland*

Received 12 March 2013; accepted in revised form 12 June 2013; Available online 22 June 2013

Abstract

Here, we present sedimentological, trace metal, and molecular evidence for tracking bottom water redox-state conditions during the past 12,500 years in nowadays sulfidic and meromictic Lake Cadagno (Switzerland). A 10.5 m long sediment core from the lake covering the Holocene period was investigated for concentration variations of the trace metals Mn and Mo (XRF core scanning and ICP-MS measurements), and for the presence of anoxygenic phototrophic sulfur bacteria (carotenoid pigment analysis and 16S rDNA real time PCR). Our trace metal analysis documents an oxic-intermediate-sulfidic redox-transition period beginning shortly after the lake formation ~12.5 kyr ago. The oxic period is characterized by low sedimentary Mn and Mo concentrations, as well as by the absence of any remnants of anoxygenic phototrophic sulfur bacteria. Enhanced accumulation/preservation of Mn (up to 5.6 wt%) in the sediments indicates an intermediate, Mn-enriched oxygenation state with fluctuating redox conditions during a ~2300-year long transition interval between ~12.1 and 9.8 kyr BP. We propose that the high Mn concentrations are the result of enhanced Mn^{2+} leaching from the sediments during reducing conditions and subsequent rapid precipitation of Mn-(oxyhydr)oxide minerals during episodic and short-term water-column mixing events mainly due to flood-induced underflows. At 9800 ± 130 cal yr BP, a rapid transition to fully sulfidic conditions is indicated by the marked enrichment of Mo in the sediments (up to 490 ppm), accompanied by an abrupt drop in Mn concentrations and the increase of molecular biomarkers that indicate the presence of anoxygenic photosynthetic bacteria in the water column. Persistently high Mo concentrations >80 ppm provide evidence that sulfidic conditions prevailed thereafter until modern times, without any lasting hypolimnetic ventilation and reoxygenation. Hence, Lake Cadagno with its persistently stable chemocline offers a framework to study in great temporal detail over ~12 kyr the development of phototrophic

* Corresponding author. Address: Geological Institute, ETH Zurich, Sonneggstrasse 5, CH-8092 Zurich, Switzerland. Tel.: +41 44 632 8731; fax: +41 44 632 1075.
E-mail address: stefanie.wirth@alumni.ethz.ch (S.B. Wirth).
[1] Present address: Institute of Geological Sciences and Oeschger Centre for Climate Change Research, University of Bern, Bern, Switzerland.

http://dx.doi.org/10.1016/j.gca.2013.06.017

sulfur bacteria communities and redox processes in a sulfidic environment, possibly depicting analogous conditions in an ancient ocean. Our study underscores the value of combining sedimentological, geochemical, and microbiological approaches to characterize paleo-environmental and -redox conditions in lacustrine and marine settings.

1. INTRODUCTION

Environmental and climatic parameters such as temperature, wind stress, catchment vegetation, primary productivity as well as water, ion and sediment supply affect the stratification of and oxidation–reduction (redox) conditions in the water column of lacustrine and marine basins. The capacity to reconstruct past bottom-water redox conditions from sedimentary records therefore yields information on paleoenvironmental and -climatic conditions. Furthermore, modern sulfidic (euxinic) lacustrine and marine basins (e.g. Lake Cadagno, Fayetteville Green Lake, Lake Pavin, Cariaco Basin, Black Sea) are often considered as analogues for ancient oceans, helping to better understand the initial ocean oxygenation and the early evolution of the biosphere (Arnold et al., 2004; Anbar et al., 2007; Canfield et al., 2008; Dahl et al., 2010a; Nägler et al., 2011). In this context, meromictic and sulfidic Lake Cadagno, with its well-defined small basin (0.26 km^2) and catchment area (2.5 km^2), is a unique natural laboratory to study variations in past redox conditions as well as related changes in the community structure of anoxygenic phototrophic sulfur bacteria. In addition, Lake Cadagno provides an ideal setting to test the applicability of various paleo-proxies in a well-studied modern aquatic system.

From a geochemical perspective, elevated molybdenum (Mo) concentrations found in lacustrine and marine sediments have been used as key evidence for sulfidic conditions in the overlying water column (Crusius et al., 1996; Nägler et al., 2005; Anbar et al., 2007; Dahl et al., 2010b; Scott and Lyons, 2012). In oxic waters, the Mo^{6+} ion occurs in the form of the conservatively behaving molybdate anion (MoO_4^{2-}). When encountering H_2S_{aq} concentrations >11 μM (Erickson and Helz, 2000), however, MoO_4^{2-} reacts to form thiomolybdates ($MoO_{4-x}S_4^{2-}$) in a series of sulfidation steps that all consume H_2S (Erickson and Helz, 2000). Tri-thiomolybdate ($MoOS_3^{2-}$) is rapidly reduced to a highly reactive Mo^{4+}-sulfide species (Vorlicek et al., 2004; Dahl et al., 2013) that is readily scavenged with either Fe-sulfides and/or organic particles in the water column, promoting efficient Mo burial (Vorlicek et al., 2004; Dahl et al., 2010a). Importantly, a common feature of all modern euxinic marine as well as open lacustrine basins is the strong enrichment of Mo in the background sediments (>25 ppm) relative to Mo concentrations in catchment rocks (typically in the range of only 1 ppm) (Dahl et al., 2010a; Scott and Lyons, 2012). This reflects the non-conservative behavior of Mo in sulfidic versus oxic settings (Emerson and Huested, 1991; Lyons et al., 2009; Scott and Lyons, 2012). Modern Lake Cadagno offers a lacustrine complement with >100 ppm Mo in the surface sediments (Dahl et al., 2010a).

Following a microbiological approach, the presence of anoxygenic phototrophic sulfur bacteria is an indicator for sulfidic, and in rare cases ferruginous (Crowe et al., 2008a), conditions in the photic zone of the water column. In modern environments, these organisms generally thrive at water-column chemoclines, where H_2S is available as electron source during photosynthesis (rather than H_2O used in oxygenic photosynthesis). Hence, the presence of their remnants (e.g. as fossil DNA and/or photosynthetic pigments) in sediments is highly indicative for past water-column euxinia in the photic zone (e.g. Brocks et al., 2005; Brocks and Schaeffer, 2008). Phototrophic sulfur bacteria can be divided into two groups, purple (PSB) and green (GSB) sulfur bacteria. GSB can cope with dimmer light conditions and are thus likely more tolerant towards environmental changes that affect light (e.g. turbidity, algal production) (Manske et al., 2005; Tonolla et al., 2005; Decristophoris et al., 2009; Meyer et al., 2011).

While Mo enrichment and biomarkers of anoxygenic sulfur bacteria within the sediments are good indicators of sulfidic conditions, elevated sedimentary manganese (Mn) concentrations are, according to the higher redox potential of Mn-oxide relative to sulfate ($O_2 > NO_3^-/NO_2^- > MnO_2 > FeOOH > SO_4^{2-} > CO_2$), indicative for a suboxic, or better 'manganous' (Canfield and Thamdrup, 2009), redox regime. On the one hand, intense Mn leaching from the lacustrine sediments induced by reducing water conditions leads to increased concentrations of dissolved Mn^{2+} in the lake's bottom water. On the other hand, fast Mn^{2+} oxidation can happen via autocatalytic reactions and/or through microbial metabolism after mixing with O_2-rich waters (Grill, 1982; Morgan, 2005; Learman et al., 2011). Such massive Mn^{2+} oxidation can eventually lead to Mn-(oxyhydr)oxide and Mn-carbonate crusts found in sediment records (e.g. Huckriede and Meischner, 1996; Bellanca et al., 1999; Sabatino et al., 2011). Sedimentary Mn enrichments through the formation and trapping of Mn-(oxyhydr)oxides and Mn-carbonates have therefore brought in association with generally anoxic depositional environments that are episodically perturbed by oxygenation events (e.g. due to eustatic sea-level change, changes in primary productivity, inflows of oxygenated waters into marine or lacustrine basins) (Calvert and Pedersen, 1996). The injection of O_2-rich waters triggers the formation of Mn-(oxyhydr)oxides in the water column. After their deposition, Mn-(oxyhydr)oxides may be transformed to Mn-carbonates in the presence of reducing anoxic sediments (Calvert and Pedersen, 1996; Huckriede and Meischner, 1996). Given the right preservation conditions, i.e. rapid burial before Mn mineral phases are reduced and Mn^{2+} released to the water column (März et al., 2011), sedimentary Mn enrichments can thus be taken as indicators of sporadic

water-column ventilation during otherwise anoxic conditions in the past.

An innovative way to determine sedimentary distribution patterns of the redox-sensitive metals Mn and Mo in lacustrine and marine sediments is to use an X-ray fluorescence (XRF) core scanner (Jansen et al., 1998; Richter et al., 2006; Hennekam and de Lange, 2012). Whereas the analysis of major elements (e.g. Al, Si, K, Fe) has been well established (e.g. Böning et al., 2007; Giguet-Covex et al., 2011), the applicability of trace-metal records, particularly of Mo in lake sediments, is only sparsely investigated. Scanning XRF analysis is non-destructive and allows a continuous assessment of the chemical composition of the sediment at very high spatial, and thus temporal, resolution. This is clearly an advantage over traditional analytical methods (e.g. ICP-AES, ICP-MS) and is helpful for the reconstruction of short-term environmental fluctuations. A disadvantage, however, is that scanning XRF analysis only yields semi-quantitative (i.e. relative) results. Hence, the absolute assessment of element concentrations by traditional ICP-MS analysis for calibration purposes is still required. The community structure of the anoxygenic phototrophic sulfur bacteria can be reconstructed using 16S rDNA real time PCR analysis (here seven Chromatiaceae (PSB) and two Chlorobiaceae (GSB) populations) as well as through carotenoid pigment (okenone and isorenieratene) analysis. The combination of elemental records from XRF core scanning with microbiological analyses thus allows for a reliable reconstruction of past water-column redox conditions, as well as of the possible environmental factors that drove potential changes in bottom water oxygenation and the phototrophic sulfur bacteria community.

The combined study of the sedimentology, chronology, and biogeochemistry of the Holocene record of Lake Cadagno allows us to assess the initiation and perpetuity of euxinic conditions in Lake Cadagno (i.e. the onset of meromixis) and to document temporal fluctuations in the stability of water-column stratification and euxinia during a time period of 10 kyrs. We demonstrate how an interdisciplinary approach can be used to constitute a high-resolution record of past redox conditions in the bottom waters of lacustrine environments with direct pertinence also to marine basins.

2. STUDY SITE

Lake Cadagno is a small (0.26 km^2) crenogenic meromictic lake located in the Piora Valley in the central Alps of Switzerland (46°33′01″N, 8°42′41″E) at an altitude of 1921 m above sea level (Fig. 1). The 21 m deep lake basin formed after glacial retreat ~12,000 years ago. Its catchment geology mainly consists of high- to ultrahigh-grade metamorphic rocks such as para- and orthogneisses, as well as amphibolites or hornblende schists (Krige, 1917). Triassic dolomite and rauwacke with some gypsum, the so-called Piora Zone, forms the southern border of the lake. Today, subaquatic springs within the Triassic rocks dipping below the lake along its southeastern part maintain a flow of solute-rich waters to the lake. This leads to a strong density gradient in the water column and a permanent stratification with an oxic mixolimnion, an anoxic monimolimnion and a chemocline at a depth of 10–13 m separating the two water bodies (Fig. 1b and c) (Del Don et al., 2001). Fig. 2 shows water profiles of dissolved O_2, H_2S, as well as of water conductivity and temperature, demonstrating the special chemical and physical properties of the Lake Cadagno water column. The chemocline hosts abundant populations of anoxygenic phototrophic green and purple sulfur bacteria (e.g. Tonolla et al., 2005; Musat et al., 2008; Gregersen et al., 2009; Habicht et al., 2011). Intense research in the field of microbial ecology and biogeochemistry has been conducted in the modern lake, targeting the water column and shallow surface sediments (e.g. Tonolla et al., 2005; Musat et al., 2008; Decristophoris et al., 2009; Dahl et al., 2010a; Peduzzi et al., 2011, 2012). These studies have shown that meromixis has prevailed in Lake Cadagno for at least the past ~100 years (Del Don et al., 2001), but the longer-term history of meromixis and redox conditions in Lake Cadagno has not been studied, and the timing of the transition from oxic to euxinic conditions in the water column is unknown.

3. MATERIALS AND METHODS

3.1. Sediment cores

Sediment cores covering the complete lacustrine record of Lake Cadagno were retrieved in September 2009 from the deepest central part of the lake. Twin cores (composite Core 1) with a vertical offset of 1.5 m were recovered as 3 m sections using an UWITEC platform with a percussion piston-coring system. In addition, undisturbed surface sediments were retrieved from the same location using a gravity corer (1 m core length). An additional Holocene single core (Core 2) dedicated to molecular biological analyses was taken from the same location.

Core 1 was transported in 1 m segments to the Geological Institute at ETH Zurich, where both the un-opened, as well as later the split cores, were stored at 4 °C in a cold room. Initial analyses in the laboratory included gamma-ray attenuation bulk density measurements at 0.5 cm resolution on un-opened cores using a multi-sensor core logger (Geotek Limited, Daventry, UK). After opening of the cores by longitudinally splitting them into halves, the sediment surface was photographed and a continuous composite core record was established. Core 2 was opened and sampled in 5 cm (gravity core) and 10 cm intervals (piston core) at the Lake Cadagno field station within 1 day after core recovery. Samples were immediately frozen and kept at −80 °C in order to prevent deterioration of pigments and microbial DNA (Niemann et al., 2012; Ravasi et al., 2012).

3.2. Geochemical analyses

Non-destructive and continuous XRF core scanning on Core 1 was performed using an Avaatech instrument (Den Burg, The Netherlands) with a rhodium (Rh) tube as X-ray source. Since XRF scanning only penetrates into the uppermost millimeter of the sediment, the sediment surface

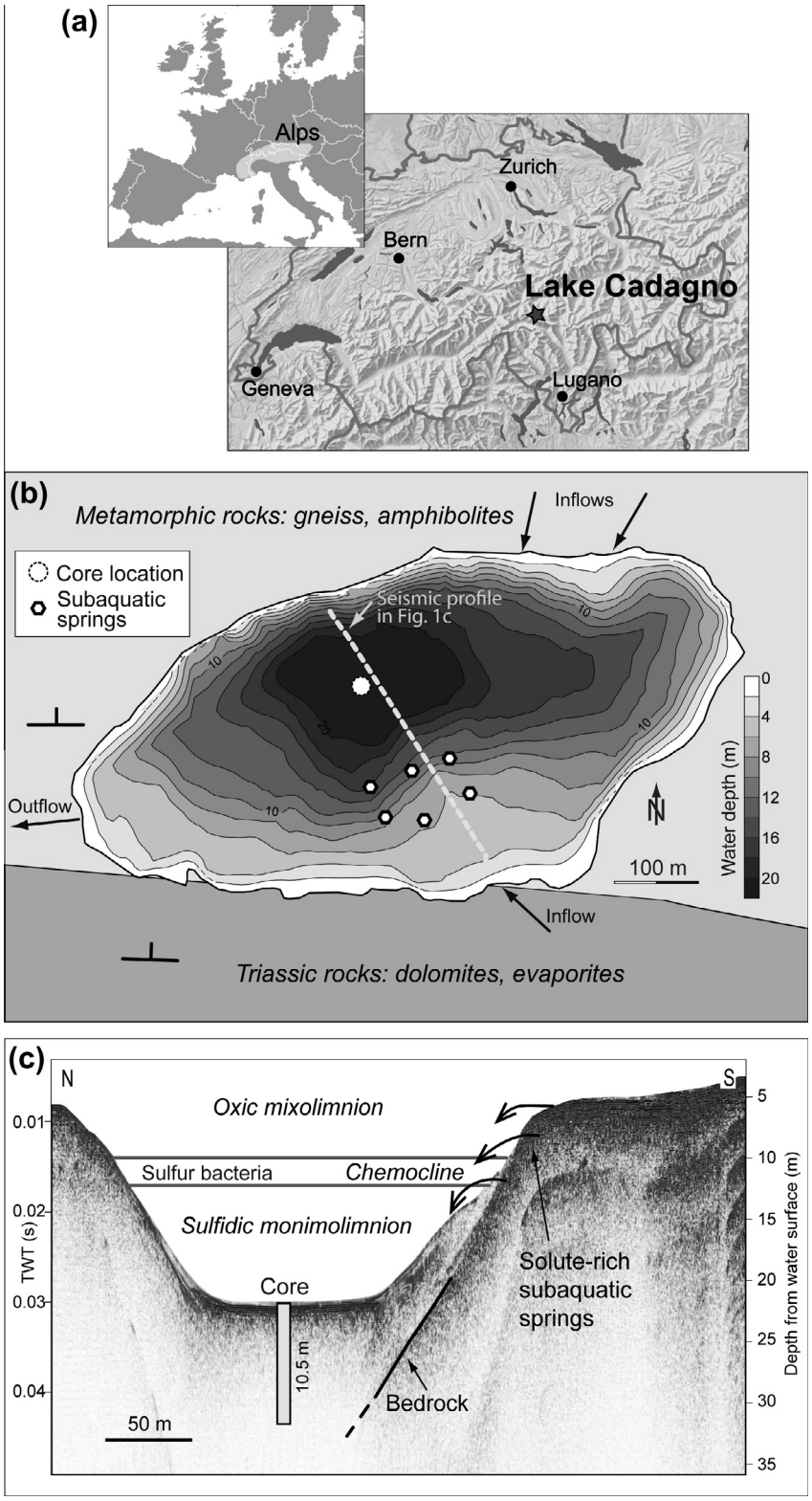

Fig. 1. (a) Geographical location of Lake Cadagno in south-central Switzerland. (b) Bathymetric map derived from reflection seismic data with surrounding catchment lithologies, sediment core location, and the position of the subaquatic springs. (c) High-resolution single-channel 3.5 kHz reflection seismic profile (location marked with white dashed line in Fig. 1b) illustrating the flat, infilled central basin floor, the sediment core length and, schematically, the stratification of the water column.

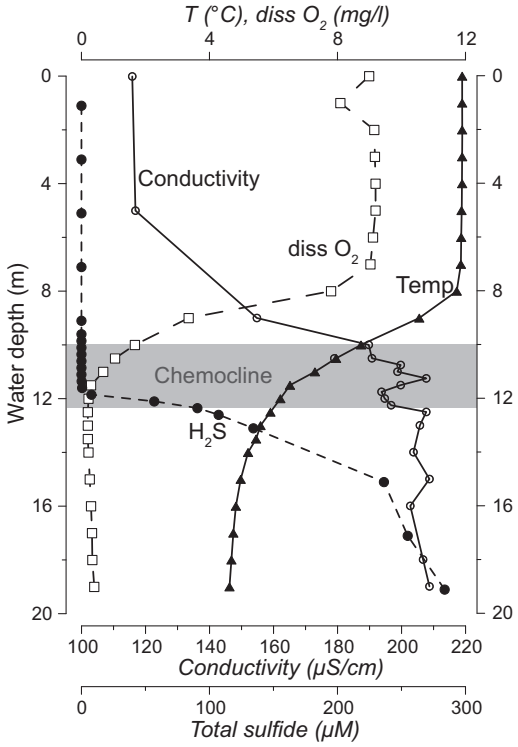

Fig. 2. Physical and chemical properties of the water column demonstrating steep gradients within and in the vicinity of the chemocline (data from Dahl et al., 2010a; measured on September 25, 2006 (dissolved O_2, H_2S) and September 27, 2006 (temperature, conductivity)). The water-column properties were measured at the location of maximum water depth close to the coring location.

was carefully cleaned and smoothed by scratching off 1–2 mm of sediment before scanning. Vertical step resolution and slit opening was 1 mm, horizontal slit opening was 12 mm (i.e. the analyzed area per scan is 12 mm^2). Exposure time was 20 s, applied current 2000 µA, and applied voltage 10 kV (for the elements Al, Si, S, K, Ca, Mn, Fe) and 30 kV (Br, Rb, Sr, Zr, Mo). Results from XRF core scanning are presented as relative down-core variability in counts per 20 s measurement duration (cts/20 s). Sediment inhomogeneity and varying physical properties, e.g. grain size and pore-water content, within the record complicate control on measurement geometry and element interactions (Richter et al., 2006; Tjallingii et al., 2007; Hennekam and de Lange, 2012) and may affect the measured pattern. Due to the fact that the largest changes in grain size and mineral content in Lake Cadagno are given by lithology alternation, a color code for visualizing the different lithologies in the figures was used to address potential biases in the XRF data.

Sediment subsamples for elemental analysis (trace metals (Mn, Mo), total carbon (TC) and total inorganic carbon (TIC)) were freeze-dried and homogenized in an agate mortar before analysis. For accurate quantification of the key elements, Mn and Mo, a calibration of the XRF core scanning results was performed, analyzing 19 discrete samples (4 mm sampling interval) as duplicates using Inductively Coupled Plasma Mass Spectrometry (ICP-MS). Precise and careful sampling (e.g. avoiding oblique layers) was crucial for calibrating XRF core scan counts because small offsets from the XRF-scanned area and targeted data interval would already weaken the calibration (Böning et al., 2007; Spofforth et al., 2008). For ICP-MS analysis, ~100 mg of sample material was digested in two heating steps using a ETHOS One microwave system (Milestone S.r.l., Sorisole, Italy): (i) digestion by adding 3 ml of HNO_3 (65%, suprapur), 3 ml HCl (32%) and 3 ml HF (40%), (ii) neutralization of HF by adding 10 ml of boric acid (5%). Finally, solutions were transferred to polyethylene flasks that were filled up with nanopure H_2O to 100 ml. 1/100 dilutions were analyzed by ICP-MS (Agilent Technologies 7500 Series, Santa Clara, CA, USA). Metal concentrations in samples were determined using a calibration curve from a multi-element internal standard and the reproducibility of the measurements, based on replicate standard and sample analysis, is better than 8%. TC and TIC were measured with a 5012 Coulometer (UIC Inc., Joliet, IL, USA) analyzing the CO_2 content generated by combustion (TC) at 950 °C and by acidification (TIC) with perchloric acid (2N), respectively. Total organic carbon (TOC) was then calculated as the difference between TC and TIC.

3.3. Molecular biological analyses

3.3.1. Analysis of photosynthetic pigments

Total lipid extracts (TLE), containing the carotenoid pigments okenone and isorenieratene and their saturated homologues, were obtained from 2 to 8 g of homogenized, freeze-dried sediment according to a modified Bligh and Dyer method (Bligh and Dyer, 1959; Elvert et al., 2003). Elemental sulfur was removed from the TLE with activated copper. The more polar constituents were partially removed by saponification and subsequent extraction of a neutral fraction, which comprises relatively apolar compounds such as hydrocarbons, long-chain ketones and alcohols, as well as carotenoid pigments. Okenone and isorenieratene, as well as their homologues with varying degrees of unsaturation, were saturated using a platinum oxide catalyzed hydrogenation reaction (e.g. Christie, 1989) prior to chromatographic analysis.

Carotenoids were identified and their concentrations semi-quantitatively measured using a GC–MS system (Thermo Scientific TRACE GC Ultra gas chromatograph equipped with a split/splitless injector and a 60 m apolar DB-5 ms fused silica column (0.25 mm inside diameter, 0.25 µm film thickness) connected to a Thermo Scientific DSQ II quadrupole mass spectrometer operated in electrospray ionization mode). The saturates perhydrookenone and isorenieratane are identifiable based on the characteristic fragmentation pattern with clear peaks at m/z 133 and at m/z 566 (M^+-CH_3OH, perhydrookenone) or at m/z 546 (M^+; isorenieretane) (Hebting et al., 2006). The magnitude of the total ion current was used to approximate the compound concentration in the sediment.

3.3.2. Sulfur bacteria DNA extraction and quantification

Total DNA was extracted from 5 g of wet sediment using the PowerMax™ Soil DNA Isolation Kit (Mobio, Carlsbad, CA, USA). Details on the procedure can be

found in Ravasi et al. (2012). For each of the sediment samples, the number of copies of 16S rDNA of nine targeted phototrophic sulfur bacterial populations (seven Chromatiaceae and two Chlorobiaceae populations) was quantified by a real-time polymerase chain reaction (real-time PCR) (Ravasi et al., 2012). The results obtained by real-time PCR were normalized to copies per μg of extracted DNA to compensate for possible variation in the extraction efficiencies between samples. For DNA analyses, fewer samples were investigated than for carotenoid pigments and samples were selected based on pigment results.

4. CORE CHRONOLOGY

The sediment sequence was dated using activity profiles of the radionuclides ^{137}Cs and ^{210}Pb (measured using high-purity Ge well detectors at Eawag, Dübendorf, Switzerland) for the past 100 years (Appleby, 2001), and by radiocarbon dating (measured at the AMS-^{14}C laboratory at ETH Zürich, Switzerland) for the Holocene record (Fig. 3).

The sampling interval for ^{137}Cs and ^{210}Pb analysis was 0.5 cm, however, only every second sample was analyzed. The resulting ^{137}Cs activity profile (Fig. 3a) clearly shows a peak at 5.5 cm core depth, which can be related to the atmospheric weapon testing in 1963, and a second peak right at the sediment surface (the uppermost 2 or 3 cm of sediment were lost during core recovery), which is caused by the Chernobyl nuclear reactor accident in 1986. The distance between the 1986 and the 1963 maxima translates into a sedimentation rate of 2.4 mm/yr for the water-rich surface sediments, a value that stands in good agreement with data from Birch et al. (1996); Fig. 6). The exponential slope of the ^{210}Pb (^{226}Ra-corrected) profile confirms this sedimentation rate with a value of 2 mm/yr.

For radiocarbon dating, only wood and terrestrial macrofossil pieces were used, preventing potential error sources due to the hard-water effect. Radiocarbon ages (Table 1) were converted to calibrated years before 1950 (cal yr BP) using the Intcal09 calibration curve (Reimer et al., 2009). Two analyzed dates were discarded because they derive

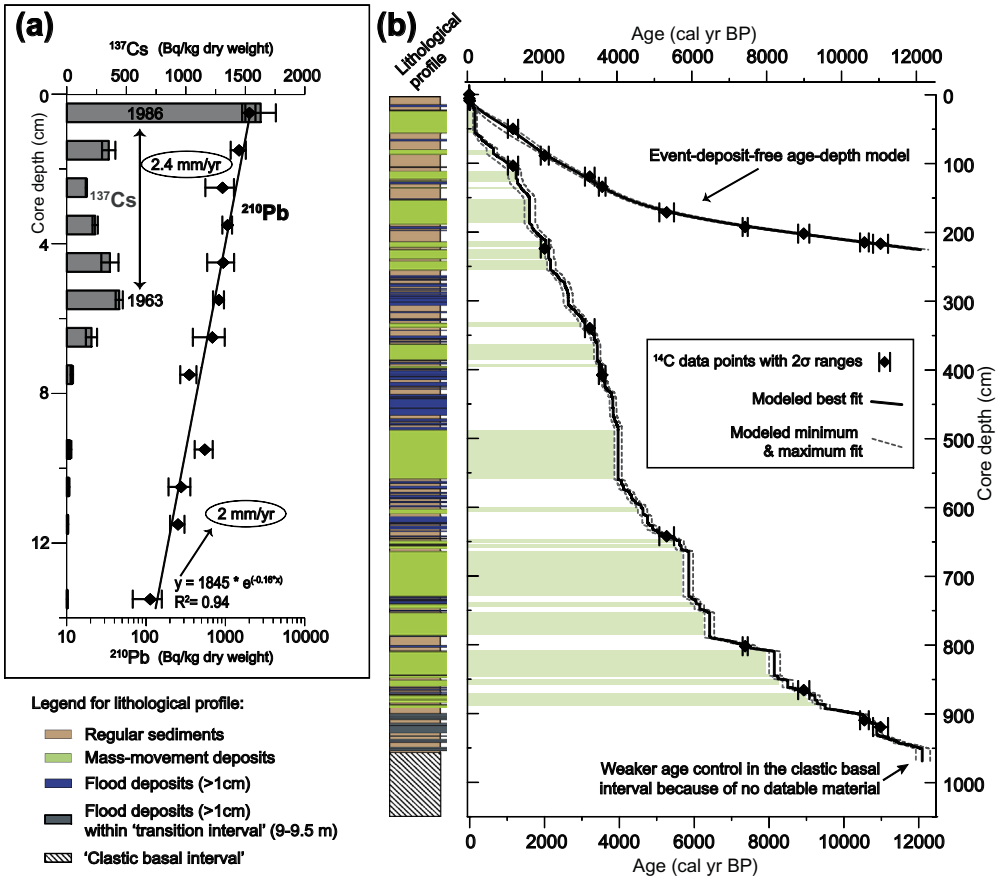

Fig. 3. (a) ^{137}Cs and ^{210}Pb (^{226}Ra-corrected) activity profiles for the uppermost 14 cm of the Cadagno sediment core. Highest ^{137}Cs activity peaks correspond to the years 1986 (Chernobyl nuclear accident) and 1963 (maximum atmospheric fallout due to nuclear weapon testing). Sedimentation rate derived from the logarithmic regression of ^{210}Pb (2 mm/yr) is in agreement with the ^{137}Cs age model (2.4 mm/yr). (b) Holocene age-depth model established on an event-deposit-free sediment sequence (upper curve) using nine radiocarbon ages and age control from ^{137}Cs dating. The lower curve includes the complete sediment succession as shown in the lithological profile on the left with event deposits plotted as vertical steps.

Table 1
Radiocarbon ages analyzed for establishing the Holocene age-depth model for Lake Cadagno Core 1.

Lab Code	Core section	Depth in section (cm)	Sample material	Comp. depth (cm)	Composite depth without event deposits (cm)	^{14}C age (yr BP)	$\pm1\sigma$	Calibrated age (cal yr BP) 2σ range
ETH-42351	CAD09-04-A1	65.5–66.5	Terr. Macrofossils	103.5	49.9	1255	60	1056–1295
ETH-39236	CAD09-04-A3	12–14	Wood	224.0	88.9	2035	35	1898–2112
ETH-41051	CAD09-09-A2	72.5–73.5	Terr. Macrofossils	339.7	119.4	3015	35	3079–3338
ETH-39237	CAD09-09-A3	43–46	Wood	407.8	134.1	3305	35	3452–3630
ETH-41052	CAD09-04-B3	92–93	Wood	642.2	171.4	4595	35	5068–5460
ETH-39238	CAD09-08-A1	31–31.5	Wood	684.2	176.0	5035	35	5663–5899*
ETH-41053	CAD09-08-A2	31–31.5	Terr. Macrofossils	776.4	183.0	8015	35	8765–9012*
ETH-42352	CAD09-05-C1	13–14	Wood	802.1	192.6	6450	35	7291–7430
ETH-41054	CAD09-08-A3	30–30.5	Wood	865.9	202.3	8055	35	8776–9079
ETH-44254	CAD09-05-C2	37.5–38.5	Terr. Macrofossils	909.7	215.1	9340	35	10431–10667
ETH-39239	CAD09-05-C2	52–55	Wood	919.6	217.0	9630	45	10776–11180

*Ages deriving from reworked material and therefore not used for age-depth modeling.

from mass-movement deposits (Table 1, marked with asterisks). Age-depth modeling with nine AMS radiocarbon ages and age control from ^{137}Cs dating (Fig. 3b) was carried out on an event-deposit-free sediment sequence, i.e. only on the record of regular sediments (see Section 5.1 for lithology classification), applying a smoothed cubic spline interpolation between the dating points using the Clam software (Blaauw, 2010). Event (i.e. short-time) deposits are presented as vertical steps (Fig. 3b).

The core chronology for Core 2 used for molecular/biomarker analyses was established by stratigraphic correlation using 68 visually determined tie points (for more information on the age model of Core 2 see Niemann et al., 2012).

5. RESULTS

5.1. Sediment lithologies

The recovered sediment record has a composite length of 10.5 m (Fig. 4). The upper 9 m consist of dark brown to blackish organic-rich deposits intercalated by mineral-rich sediment layers. Between 9 and 9.5 m core depth, the section to which we refer as 'transition interval' in the following text, the sediment facies is characterized by an increasing amount of clastic material and organic-rich deposits occur less frequently. From 9.5 m core depth to the base of the retrieved record, grey clastic sediments with very low organic content dominate (referred to as 'clastic basal interval').

Based on sedimentological observations on sediment color, layer thickness, grain size and deformation structures, the Lake Cadagno sediments were categorized into three lithologies: (i) regular authigenically-produced lacustrine sediments, from here on referred to as 'regular sediments', consisting to large parts of bacterial remains, (ii) flood deposits (FD) and (iii) mass-movement deposits (MMD). The record of regular sedimentation is frequently interrupted by the intercalation of event deposits (i.e. FD and MMD). Flood deposits are characterized by a high fraction of mineral grains and contain almost exclusively terrestrial organic material and barely any lacustrine components. The sediments mostly consist of coarse silt to sand with only faint grading, except for prominent clay caps on top of each layer. Flood layers show thicknesses from sub-mm to 13 cm. Mass-movement deposits, in contrast, are characterized by a rough overall grading from sandy particles at the base to organic-rich and silty to clayey sediments at the top and can be as thick as 70 cm. In addition, they show characteristic features such as deformation structures (oblique, disrupted and upside down-oriented segments) and enclosed mud clasts.

The elemental record established by XRF core scanning provides information on the distinct chemical composition of the three lithologies (Fig. 4). Regular sediments are best distinguished from event deposits by their high abundance of Mo and Br. In contrast, flood layers appear to be richer in detrital elements such as Al, Si, K, Ti, Rb, Zr and partly Ca, underscoring their high mineral content. Elevated sediment density also seems indicative of event layers and additionally allows distinguishing them from background sediments. Mass-movement deposits are characterized by a mixed chemical composition, containing high amounts of detrital elements but also elements that are typically found in the regular sediments (Mo, Br).

Flood layers provide paleoclimatic information since they are diagnostic of past flood events. Mass-movement deposits, on the other hand, represent mobilized, mixed and redeposited sediments from shallower parts of the lake that were transported to the deepest lake area. Hence, these deposits are out of chronological sequence with the over- and underlying sediments and are therefore not considered for paleo-climatic and -environmental reconstructions. Potential trigger mechanisms that led to slope failures are overloading of the lake delta and/or earthquake-induced shocks (e.g. Schnellmann et al., 2002; Girardclos et al., 2007; Wirth et al., 2011). Based on the decreasing kinetic energy of turbiditic underflows when reaching the flat deep basin (Mulder and Alexander, 2001; Gilli et al., 2013), the deposition of the event material is likely non-erosive and a continuous sediment succession can be assumed.

5.2. Correlations of XRF core scanning elements and quantitative calibration of Mn and Mo XRF core scanning counts

Organizing the elemental records acquired by XRF core scanning in a correlation matrix offers an overview on the elemental associations and facilitates further discussion of sediment sources (Table 2). For reasons provided above, mass-movement deposits are excluded from the analysis. Four elemental groups were defined (see Table 2): (1) Detrital/clastic elements (Al, Si, K, Ca) mainly occurring in flood layers. Linear regression reveals strong correlations among Al, Si, K ($R^2 = 0.91$–0.96) and a somewhat weaker correlation between Ca and Al, Si, or K ($R^2 = 0.53$–0.58) (Table 2). The reduced co-variance between Ca and the other detrital elements illustrates its two possible origins; it partly derives from the crystalline rocks in the vicinity of the lake (amphibolites, feldspars) and partly from the dolomitic bedrock, delivered through the subaquatic springs to the hypolimnion as Ca^{2+} ions. (2) Elements derived from the

Table 2
Correlation coefficients for selected elements analyzed by XRF core scanning for regular sediments and flood deposits. Groups 1 to 4 refer to classification according to the lithological occurrence of the elements or to their chemical behavior (see Section 5.2). Shaded fields indicate correlation coefficients higher than 0.9 (dark grey), higher than 0.5 (intermediate grey) and higher than 0.4 (light grey). Note that Fe and Mn do not show a strong correlation to any other element.

	Al	Si	K	Ca	Sr	S	Mo	Br	Fe	Mn
Mn										*1*
Fe									*1*	-0.07
Br								*1*	-0.27	0.05
Mo							*1*	0.57	-0.16	0.00
S						*1*	0.24	0.09	0.11	-0.24
Sr					*1*	0.27	0.15	0.15	0.23	-0.13
Ca				*1*	0.04	0.23	-0.50	-0.63	0.28	0.06
K			*1*	0.53	-0.25	-0.30	-0.40	-0.50	0.26	0.28
Si		*1*	0.91	0.52	-0.35	-0.20	-0.38	-0.48	0.09	0.21
Al	*1*	0.96	0.95	0.58	-0.30	-0.22	-0.44	-0.55	0.20	0.21
	Al	Si	K	Ca	Sr	S	Mo	Br	Fe	Mn
	Group 1				*2*		*3*		*4*	

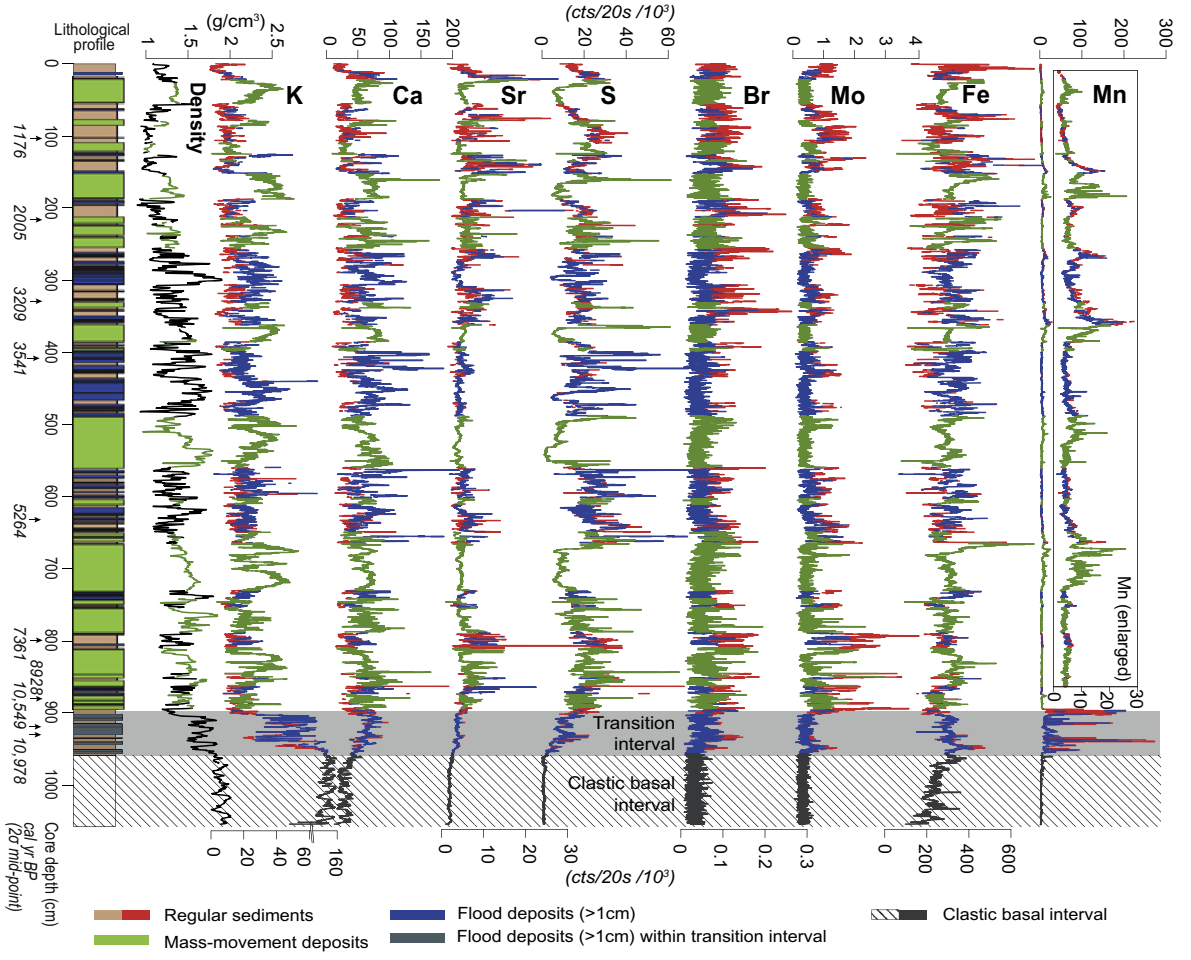

Fig. 4. Lithological profile, density record and XRF core scanning results of most relevant elements presented against sediment depth. For the density profile, regular sediments and flood deposits are not distinguished because vertical resolution (0.5 cm) is too low to properly detect flood deposits. All XRF results are given in cts/20 s/10^3. K is chosen for representation of the group of clastic/detrital elements (Al, Si, K, Ti, Rb, Zr).

subaquatic-spring water (S, Sr), without clear association with the regular sedimentation or with flood-layer deposition. (3) Elements mainly occurring in regular sediments (Mo, Br), associated with aquatic organic matter and displaying an anti-correlation with the detrital elements. Indeed, it has been shown for marine sediments that Br correlates with the amount of aquatic organic matter (Ziegler et al., 2008; Cartapanis et al., 2011). (4) Elements without any considerable correlation to the other elements and not attributable to a specific lithology (Mn, Fe). Given the lack of any obvious links to the other elements (element groups 1–3), and given the biogeochemical reactivity of these elements, they could be involved in redox and diagenetic recycling processes within sediments and pore waters, offsetting any potential source-related connection to the other elements.

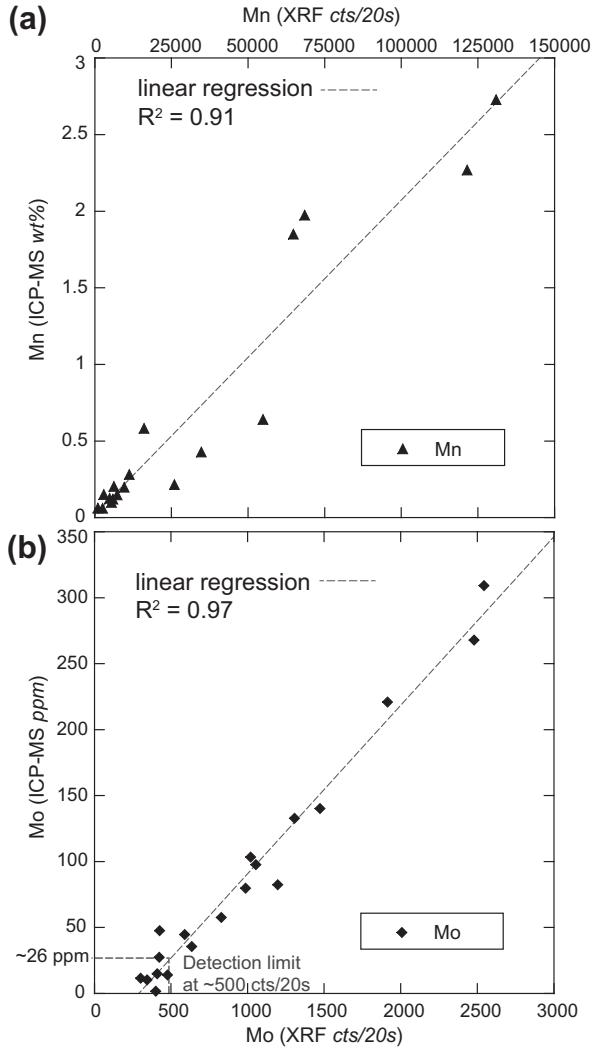

Fig. 5. Quantitative calibration of XRF core scanning counts by ICP-MS measurements for the heavy metals (a) Mn and (b) Mo. Dashed lines show linear regressions of the correlation. For Mo, the detection limit of the XRF core scanner is determined at ~26 ppm, corresponding to ~300–500 cts/20 s using a 12 mm^2 window.

The XRF core scanner results of Mn and Mo were calibrated using ICP-MS (19 samples). The correlation between the two methods was excellent, with high linear regression factors R^2 of 0.91 and 0.97 for Mn and Mo, respectively (Fig. 5). Based on this calibration we estimated the Mo detection limit for the Avaatech XRF core scanner at ~26 ppm with the applied instrument settings, corresponding to the noisy baseline at 300–500 cts/20 s (Figs. 4, 6a and 7). The manufacturer has not indicated a detection limit for Mo. In case of Mn, the detection limit of 100 ppm (declared by the manufacturer) was not reached (no noisy baseline and good absorption signal in the data).

5.3. Holocene elemental evolution

Fig. 6a shows graphs of sedimentary K, Mo, Mn, S, Ca and Fe as a function of time for the Holocene period. Regular sediments are shown in red, flood layers in blue. Although the deposition of flood layers takes place over a period of a few days at most, these deposits are attributed with an extended sedimentation time of 5 years in order to make them better visible in the XRF graphs. Mass-movement deposits are excluded from the XRF graphs in Fig. 6a, as they do not provide any paleo-environmental information in this context. Temporal resolution of the XRF data in the regular sediments ranges from 1.0 yr/mm in the recent non-compacted sediments to 15.9 yr/mm in the early Holocene. Below, we focus on features in the profiles that are most relevant for the discussion of the record in the context of paleoclimatic and -environmental change.

K – Potassium is representative of the group of clastic/detrital elements that also includes Al, Si, Ti, Rb and Zr. Highest K concentrations are observed within flood layers. The time period between 4.8 and 2.3 kyr BP is characterized by a particularly high frequency of K peaks. In contrast, XRF data for early and late Holocene sediments reveal comparatively few K peaks.

Mo – The first elevated Mo signal occurs at ~12.1 kyr BP and concentrations increase further until 9.8 kyr BP, accompanied by rising TOC content (Fig. 7). Mo concentrations are highest right after the transition interval from 9.8 to 6.4 kyr BP within regular sediments (2000–4000 cts/20 s, >200 ppm; maximum: 4095 cts/20 s, 490 ppm). Concentrations decline afterwards to lower levels (~80–200 ppm, still significantly above detection limit), except for some peaks around 2.2 kyr BP and slightly elevated values between 1500 and 500 cal yr BP. Within flood layers, Mo counts are generally low and mostly below detection limit.

Mn – Extremely high Mn counts (up to 2.7×10^5 cts/20 s corresponding to ~5.6 wt%), are observed in the transition interval between 12.1 and 9.8 kyr BP right after the end of the period of high, glacially-induced detrital input. Elevated Mn concentrations in this interval are accompanied with substantial carbonate content (Fig. 7). After 9.8 kyr BP, the Mn profile displays reduced variability, with count rates clustering around 5000 cts/20 s (~0.1 wt%). Exceptions are five short-term 'Mn excursions' (Fig. 6a, white and black asterisks) right above mass-movement deposits or sections with abundant flood layers.

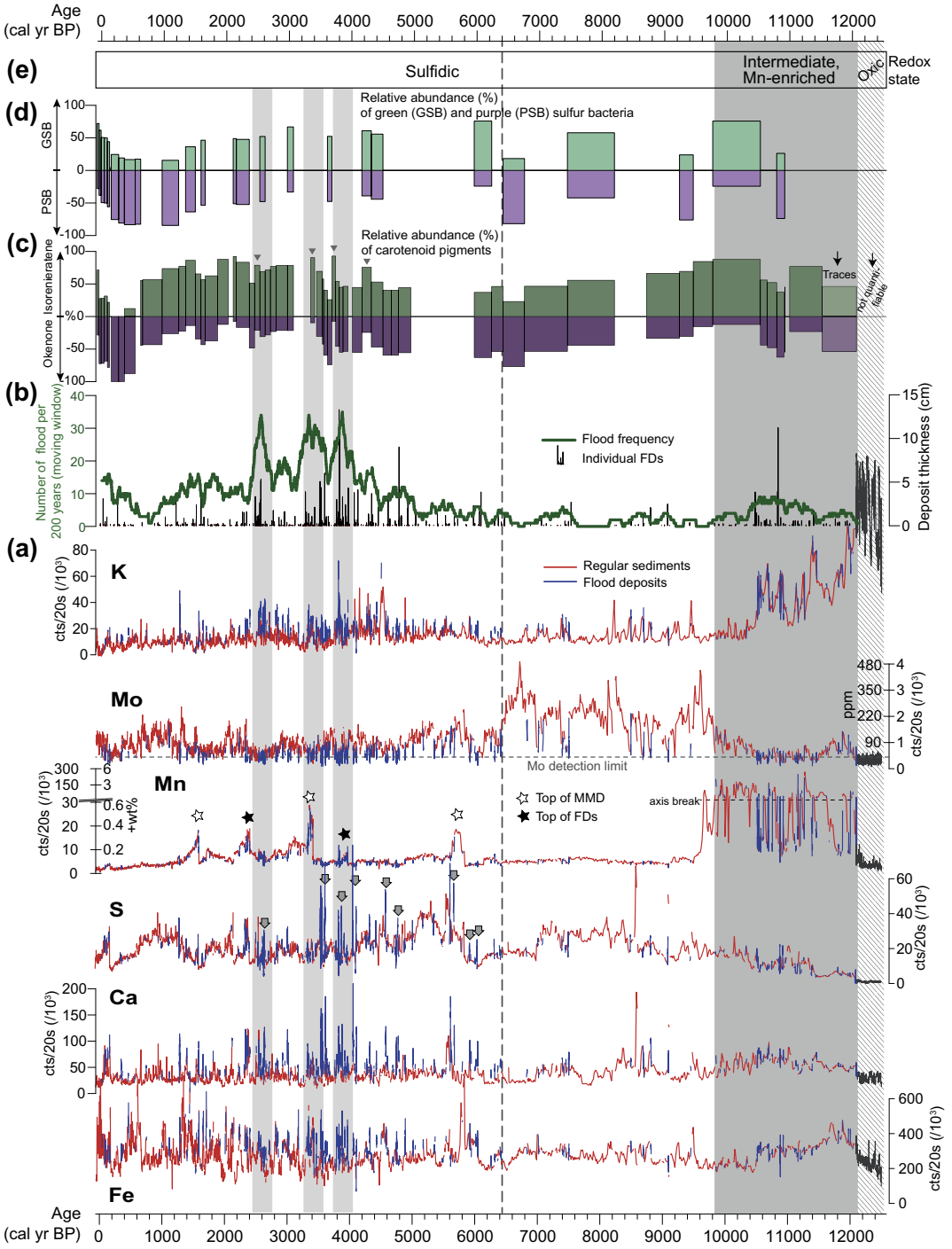

Fig. 6. Holocene evolution of (a) elements K, Mo, Mn, S, Ca and Fe, (b) flood frequency, (c) relative abundance of isorenieratene and okenone based on carotenoid pigment analysis, (d) relative abundance of green (GSB) and purple (PSB) sulfur bacteria species from 16S rDNA extraction, and (e) redox-state indication. In (a), regular sediments are plotted in red and flood deposits in blue. Although flood deposits are deposited within few hours to days, they are plotted with a duration of 5 years in order to make them visible in the graphs. For Mn and Mo, results from quantitative calibration are given in wt% (Mn) and ppm (Mo) in addition to XRF core scanning counts. Stars highlight peaks of Mn during the euxinic period, grey arrows mark flood deposits with peaks in S, Ca and Fe. In (b), the green line presents the number of flood events per 200 years, black vertical bars indicate the thickness of individual deposits. In (c) and (d), the relative abundances of isorenieratene (GSB) vs. okenone (PSB), as well as of GSB vs. PSB species is shown as positive vs. negative percentages, respectively.

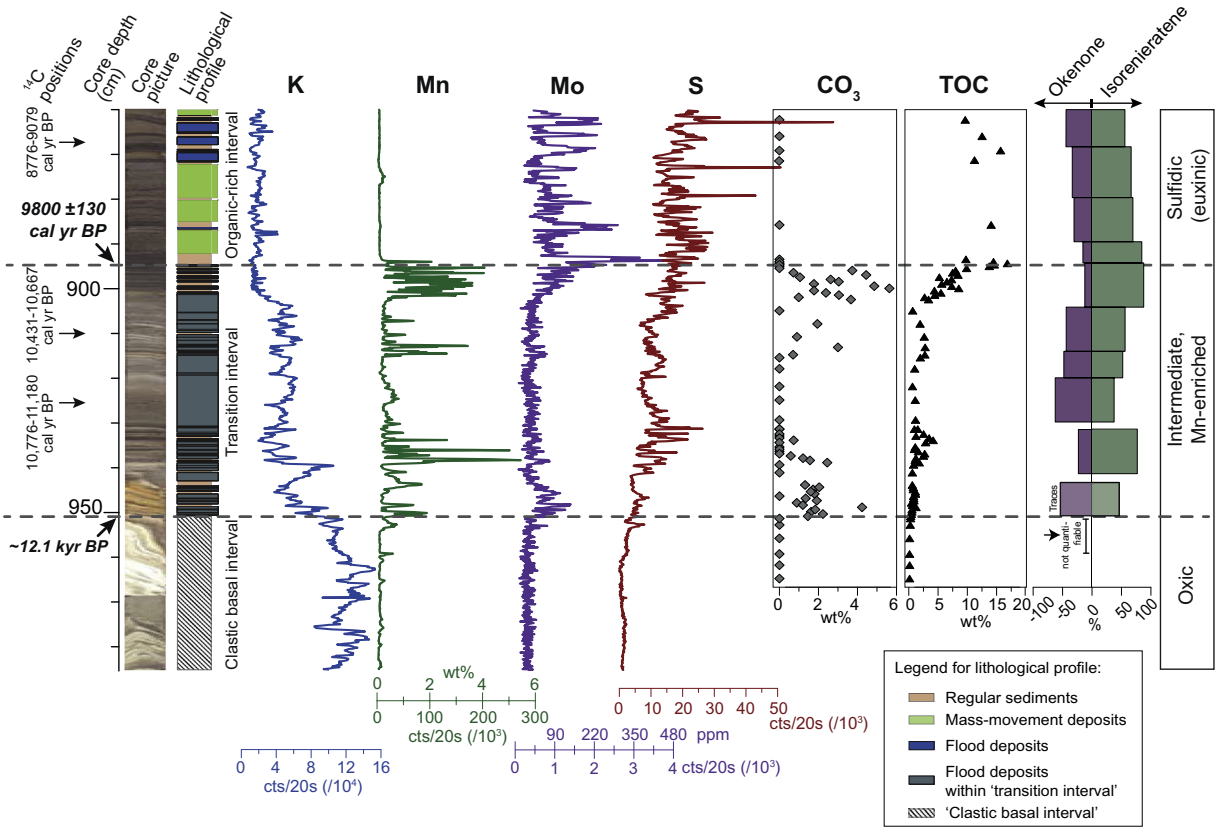

Fig. 7. Oxic-intermediate-sulfidic transition zone in the early Holocene highlighting the onset of sulfidic conditions at 9800 ± 130 cal yr BP. The lithological and K profiles illustrate the general change from clastic-dominated sediments to sediments richer in authigenic, i.e. organic (see TOC), components. The intermediate, Mn-enriched stage is characterized by elevated concentrations of Mn and carbonate, first detectable signals of Mo and an increase in S. The euxinic stage shows a sudden drop in Mn but strongly increased Mo and TOC concentrations. The presence of carotenoid pigments (shown as the relative abundance of isorenieratene vs. okenone as positive vs. negative percentages) confirms intermittent sulfidic conditions with the onset of the intermediate, Mn-enriched phase.

S – Total S content steadily increases from 12 to 7 kyr BP, with little variation between regular sediments and flood layers, followed by a period with reduced S sedimentation between 7 and 6 kyr BP. After 6 kyr BP, S contents display fluctuations that seem to follow patterns in the Mo profile in the regular sediments. Flood layers are often associated with high S content, in particular around 5.6 and between 4.2 and 3.4 kyr BP (Fig. 6a, grey arrows).

Ca – As mentioned above, Ca has a bimodal behavior due to its dual-source character. In general, it correlates quite well with K, but shows additional high-amplitude peaks in the flood layers, coinciding with the high-amplitude S peaks.

Fe – Fe contents show little variation in the early Holocene, but becomes quite variable after 6 kyr BP, particularly in flood layers between 4 and 3.2 kyr BP, but also in the regular sediments of the last 2 kyr. No correspondence to K or S is observed.

5.4. Temporal distribution of flood layers

A flood frequency curve, indicating the number of floods occurring in a 200-year moving interval is presented in Fig. 6b. Flood frequency appears to be moderate in the early Holocene between 12 and 10.3 kyr BP. However, caution is advised when interpreting this part of the flood-deposit record with regards to paleo-flood reconstructions. Particularly in the early phase of lake evolution, after the retreat of the glacier, a substantial fraction of the detrital input likely derived from a large volume of loose material in the catchment. The missing soil and vegetation cover at that time probably facilitated erosion and transport of this material to the lake. The following four millennia (10.3 to 6.4 kyr BP) are characterized by very low or absent flood activity. After 6.4 kyr BP, the flood frequency increases, reaching highest values at 3.8, 3.2–3.5 and 2.5 kyr BP. Thereafter, flood-frequency values decrease significantly in the time period 2 to 1 kyr BP and return even to early-Holocene levels between 1000 and 500 cal yr BP. Towards modern time, the sediment record suggests yet another increase in flood frequency.

5.5. Molecular biological records

Carotenoid pigments (okenone and isorenieretane) were successfully detected in quantifiable amounts in all analyzed samples, only the two oldest samples contained no (~12.5–12.1 kyr BP) or only trace amounts (~12.1–11.6 kyr BP) of the target pigments (Fig. 6c). Phototrophic sulfur bacterial DNA was likewise successfully extracted from all analyzed

samples (Fig. 6d). Out of the seven Chromatiaceae populations analyzed for DNA six contain okenone and only one, *Lamprocystis roseopersicina*, rhodopinal (Peduzzi et al., 2011, 2012). Presently (1990–2012), *L. roseopersicina* is found at very low numbers in the water column and therefore constitutes a minor fraction of the total Chromatiaceae population (Tonolla et al., 2005). Both investigated Chlorobiaceae produce isorenieratane. Results from lipid biomarker and DNA analysis are therefore expected to similar results. Indeed, both records show a consistent pattern (Fig. 6c and d). In the early Holocene (10.5–8 kyr BP) GSB show a weak dominance. The middle Holocene is characterized by a rather weak prevalence of PSB. Concomitantly with the rise in flood frequency (<5 kyr BP), the relative abundance of GSB increases again. Here, the two isorenieratene peaks at 3.7 and 3.4 kyr BP seem to correspond to flood-frequency highs with a time lag of roughly 50–100 years (e.g. at 4.3, 3.8, 3.4 and weakly at 2.5 kyr BP). PSB become more abundant during the period of low flood activity between 1500 and 500 cal yr BP. However, with increasing flood activity towards the present, the bacterial community structure is again shifted towards GSB dominance.

6. DISCUSSION

6.1. Onset of euxinia at 9800 ± 130 cal yr BP and associated behavior of Mn and Mo

The basal part of the retrieved sediment record between 9.8 and 8.8 m core depth (i.e. between 12.5 and 9 kyr BP) reveals distinct changes in sediment lithology and color as well as in chemical composition (Fig. 7). We interpret this section in the context of an oxic–sulfidic redox transition period in the very early Holocene. The overall cause for the onset of sulfidic conditions can most likely be attributed to climate warming after the last glacial termination. Warming led to permafrost melting, thus activating the subaquatic springs that fuel the lake with solute-rich water. In addition, the development of vegetation and soils after glacier retreat (Bernasconi et al., 2011; Thevenon et al., 2012), and the consolidation of loose sediments in the catchment, decreased the frequency and intensity of sediment-laden underflows (reflected in the decrease in clastic material at ~893–900 cm core depth; Fig. 7). Less frequent (flood-induced) underflows, i.e. processes that tend to mix the water column, in combination with the activation of the subaquatic springs provided environmental conditions that were conducive to the formation and sustainment of a stable chemocline. In the following, we discuss in detail the geochemical behavior of Mn and Mo during oxic, intermediate and sulfidic redox regimes in the Lake Cadagno water column, providing supporting evidence for the early redox transition into euxinia that has prevailed until today (Fig. 8).

6.1.1. Oxic conditions (Fig. 8a)

During oxic (i.e. well-mixed water column) conditions (time of lake formation about 12.5 kyrs ago to ~12.1 kyr BP) Mn reached the lake with the detrital inflow and was present in the water column as dissolved unstable Mn^{2+} or as oxidized, particulate Mn-(oxyhydr)oxides (Davison, 1993). It is reasonable to assume that even at those times the sediment–water interface and the sediments were reducing, so that Mn-(oxyhydr)oxides are reduced to Mn^{2+}, which then diffuses back into the water column (Froelich et al., 1979; Huckriede and Meischner, 1996; Schaller and Wehrli, 1997). Released Mn was reoxidized and reprecipitated in the water column, and/or washed out of the lake as suspended particles with the riverine outflow. This highly dynamic behavior of Mn has also been documented for coastal sediments where Mn is recycled by redox processes 100–300 times before final deposition and burial in the sediments (Canfield et al., 1993). Carbonate phases did not significantly contribute to the sediment matrix during oxic water column conditions (Fig. 7). This reflects a low availability of ions for carbonate mineral formation (Ca^{2+}, Sr^{2+}, HCO_3^-), presumably because the subaquatic springs were not yet active and alkalinity was insufficient to induce carbonate precipitation. In the absence of sulfate input as well as of large amounts of organic matter,

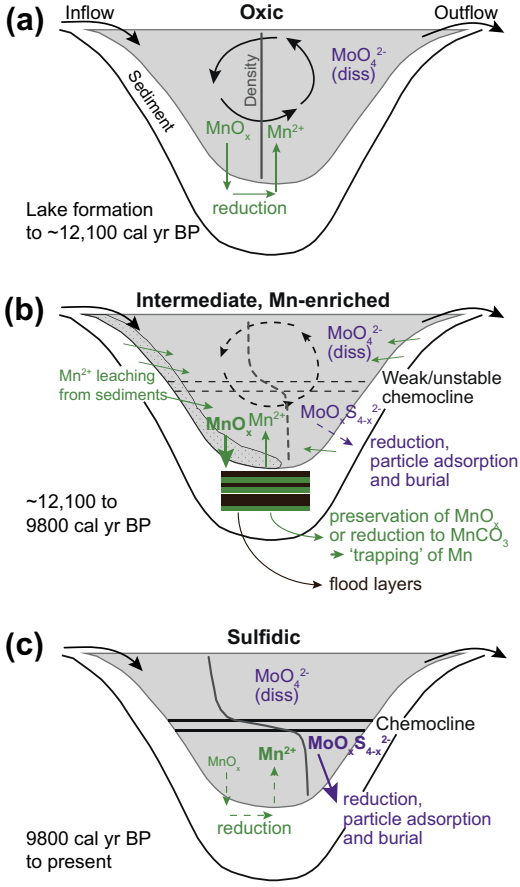

Fig. 8. Models for Mn and Mo behavior during the three distinct redox stages (a) oxic, (b) intermediate, Mn-enriched, and (c) sulfidic in relation to water-column stratification and chemocline formation. Dashing and thickness of lines and arrows, as well as bold fonts, are proportional to intensity and stability of reactions and processes. In (b), a flood-induced underflow is schematized, delivering O_2-rich water to the lake bottom and triggering the precipitation of Mn-(oxyhydr)oxides, with subsequent preservation of Mn mineral phases in between the flood layers.

and prior to the onset of density stratification of the water column, respiratory sulfate reduction was likely of minor importance and sulfide levels in the water column must have remained below the H_2S_{aq} threshold (>11 μM) for thiomolybdate formation, which is the prime requisite for intense sedimentary Mo enrichment. Mo likely remained in the oxic water column as dissolved MoO_4^{2-}, and since Mo concentrations in the catchment rocks (~0.5 ppm) and in the dissolved Mo load of the riverine inlet (~8 nmol/kg) are low (Dahl et al., 2010a), we expect Mo-poor sediments with concentrations (~1 ppm) well below detection limit of the XRF core scanner.

6.1.2. Intermediate, Mn-enriched conditions (Fig. 8b)

An intermediate/fluctuating redox state is inferred from ~12,100 to 9800 cal yr BP, recording high-amplitude and short-term fluctuations of Mn (Fig. 7). At the beginning of this period, substantial S, Sr and Ca counts suggest that the subaquatic springs have been activated at this time. Supply of salt-rich spring waters thus led to the formation of a density gradient and therefore an initial weak stratification in the water column.

As a consequence of density stratification, conditions in the bottom waters must have become more reducing, enabling enhanced Mn^{2+} leaching from the lacustrine sediments affected by reducing water conditions as well as Mn^{4+} reduction in the water column, leading to a high Mn^{2+} retention in the anoxic water body (Huckriede and Meischner, 1996). Due to this high Mn^{2+} concentration, Mn-(oxyhydr)oxides precipitated to large extents where and when oxic and anoxic waters mixed (Fig. 9b) (Huckriede and Meischner, 1996; Löwemark et al., 2008). Mixing events were most likely associated with flood events injecting dense, sediment-loaded and O_2-rich waters to the lake bottom and destroying or disturbing the weak stratification by underflows. We argue that Mn oxidation and burial happened fast, supported by an autocatalytic oxidation effect and, possibly more important, biotic catalysis (Grill, 1982; Morgan, 2005; Learman et al., 2011). Indeed, during this redox transition interval, the sedimentary TOC content increased (beginning ~12,100 cal yr BP, at 950 cm core depth; Fig. 7), suggesting higher nutrient availability and primary productivity in the photic zone or perhaps enhanced organic carbon preservation. Furthermore, it is reasonable to assume that the enhanced input of alkaline anions to the lake promoted the precipitation of carbonate minerals. The coincidence of high Mn peaks with subtle Ca peaks in the XRF data suggests the occurrence of Mn–Ca-carbonates (Middelburg et al., 1987) that formed in the mildly reducing water column, where Mn^{2+} co-precipitates with the carbonates at a relatively high pH, or by reduction of Mn-oxyhydroxides after deposition (Calvert and Pedersen, 1996; Huckriede and Meischner, 1996). The fact that Mn-(oxyhydr)oxides that formed in the oxic water column did not undergo reduction to Mn^{2+} before being deposited, distinguishes this intermediate, Mn-enriched redox phase in Lake Cadagno from ferruginous conditions. Such conditions can presently be found in Lake Matano, an accepted modern analogue for Archean and early Proterozoic oceans (Canfield et al., 2008), where Mn-oxides are reduced in the water column before reaching the lake floor (Jones et al., 2011).

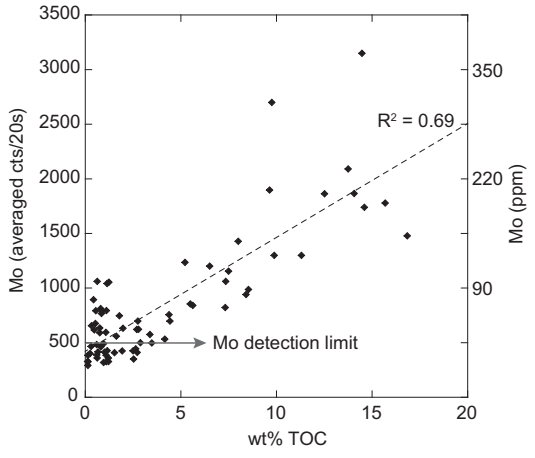

Fig. 9. Linear relation between Mo and TOC content during the oxic-intermediate-sulfidic transition period (with a slope of ~14 ppm Mo/wt% TOC), indicating the relevance of organic material for Mo burial. Mo XRF counts are averaged over the TOC sampling interval. For positions of TOC samples see Fig. 7.

The long-term preservation of Mn mineral phases that were precipitated during this intermediate redox period requires specific environmental conditions. We propose that the initial precipitation and deposition of Mn-(oxyhydr)oxides when O_2 is introduced to the bottom waters by flood-generated underflows leads to the formation of a Mn-(oxyhydr)oxide 'cap' or 'crust' on the sediment surface, preventing Mn^{2+} to escape from the lower sediments (Canfield et al., 1993). In addition, we propose that the subsequent rapid burial by flood-borne sediment material shields the Mn layers from reducing conditions at the sediment–water interface. Measured carbonate concentrations (Fig. 7) suggest that part of the Mn-(oxyhydr)oxides were transformed to Mn-carbonates after deposition, consistent with models proposed by Calvert and Pedersen (1996) and Huckriede and Meischner (1996). The good preservation of the Mn layers in the Lake Cadagno sediments is probably warranted/supported by the 'trapping' in between flood layers. Due to their low organic carbon content, they provide a less reducing milieu, where aerobic conditions after ventilation events are likely maintained for a longer period than would be the case for organic-rich sediments.

There is evidence that the hypolimnion was already intermittently sulfidic during this Mn-enriched state. Molecular biomarker and DNA extraction show that green and purple sulfur bacteria thrived in the water column, and high Mo concentrations sporadically reaching 40–90 ppm reflect the presence of >11 μM H_2S that is required to form particle reactive Mo species (Vorlicek et al., 2004; Dahl et al., 2013), which adsorb onto Fe-sulfides and/or organic particles settling into the sediments (Bostick et al., 2002; Helz et al., 2004, 2011; Dahl et al., 2010a). Hence, the rising TOC content in the regular sediments during this intermediate redox state (Fig. 7) stands in good agreement with increasing Mo concentrations (Fig. 7; Mo-TOC relation presented in Fig. 9). Nevertheless, permanently sulfidic

conditions could not yet fully develop, since stratification of the water column was often interrupted by the above-described mixing events inducing sediment-laden and O_2-rich waters to the hypolimnion. Based on the dating of the clastic flood layers between 950 and 900 cm core depth (11,950 to 10,350 cal yr BP) (Fig. 7), these oxygenation events occurred on average every 37 years. Sulfidic conditions during this period of the lake history could thus develop over a time period of a couple of decades, before the full development of euxinia was interrupted again by the intrusion of O_2-rich waters.

6.1.3. Sulfidic conditions (Fig. 8c)

At 9800 ± 130 cal yr BP the water-column stratification stabilized and the chemocline was fully developed. In the anoxic bottom waters, Mn-(oxyhydr)oxides undergo quantitative reduction to Mn^{2+}, explaining the low sedimentary Mn concentrations (Fig. 7), as well as the high Mn^{2+} concentrations in the bottom waters as presently observed (Tonolla et al., 2004). Sulfidic conditions are also indicated by the disappearance of stable carbonate phases. Reducing conditions, as well as a decreasing pH due to increasing H_2S production ($=H^{+\cdot} + HS^-$), either inhibited carbonate precipitation in the sulfidic waters or carbonate phases were post-depositionally dissolved in the sediments. Simultaneously with the drop in Mn concentrations, Mo reached its highest levels (up to ~490 ppm), providing additional conclusive evidence for sulfidic conditions in the water column. Mo-transfer from the sulfidic water column to the sediments occurred through the sulfidic Mo enrichment process (as described in Section 1) that requires H_2S_{aq} concentrations >11 μM in the water column and is also today observed in Lake Cadagno (Dahl et al., 2010a). Mo might also adsorb onto Mn-oxides in the oxic part of the water column. However, the absence of any correlation between sedimentary Mn and Mo rules out Mn-oxides as final Mo-shuttle (Goldberg et al., 2012; Scott and Lyons, 2012) all the way to the Lake Cadagno sediments and rather suggests that they are already reduced to Mn^{2+} in the sulfidic water column.

6.2. Holocene redox-state and chemocline evolution

6.2.1. Persistent but variable euxinia: evidence from Mo and sulfur bacteria remnants

After initial development ~9800 years ago, sulfidic conditions in Lake Cadagno prevailed to the present time. Most important evidence for persistent euxinia in the water column are (1) lasting Mo concentrations above ~80 ppm in the regular sediments (Nägler et al., 2005; Anbar et al., 2007; Lyons et al., 2009; Dahl et al., 2010b; Scott and Lyons, 2012), and (2) the presence of photosynthetic sulfur bacterial pigments and DNA throughout the record.

Although euxinic conditions prevailed, we find evidence for variations in the strength of euxinia in the Lake Cadagno water column. We determine the highest Mo burial rates, i.e. the most reducing conditions, during the early Holocene (9.8–6.4 kyr BP), accompanied by a trend from a GSB- to a PSB-dominated bacteria community and corresponding to a period of strongly reduced flood activity (Fig. 6). The subsequent decrease in Mo after 6.4 kyr BP is paralleled by an increasing abundance of GSB and an enhanced flood frequency. We hypothesize that frequent flood events sporadically ventilated the bottom waters, bringing oxygen-laden waters to the hypolimnion and periodically interrupting the molybdate-sulfidation reaction. At the same time, frequent flooding increases turbidity and possibly nutrient availability in the water column. Enhanced light absorption due to higher suspended particle concentrations and algal/cyanobacterial growth in the surface and subsurface waters thus likely reduced light availability within the chemocline. Since GSB are known to be more low-light tolerant than PSB (Biebl and Pfennig, 1978; Brocks and Schaeffer, 2008), this could have triggered the observed shift in the bacterial community from a PSB to a GSB dominated population (Fig. 6c). Between 1500 and 500 cal yr BP, flood frequency decreased, while the Mo burial rate again increased and PSB regained dominance. This suggests less intense euxinia than during the initial phase in the early Holocene (9.8–6.4 kyr BP), when flood activity was comparatively low and Mo concentrations reached distinctly higher levels.

Variations in carotenoid pigment concentrations have been used to reconstruct variations in the depth of the chemocline (Itoh et al., 2003), yet this exercise is complicated and still debated (Meyer et al., 2011). An increase of GSB abundance in the sediment record may implicate a deepening of the chemocline, as the GSB better cope with lower light availability (Manske et al., 2005). However, this seems to be inconsistent with a potential rise of the chemocline due to injections of O_2-rich waters by turbidity currents (De Cesare et al., 2006). Alternatively, as described above, we provide putative evidence that the sulfur bacteria community sensitively responded to an increased occurrence of floods and/or mass-movement events because these events likely altered the nutrient supply and increased water turbidity. High light absorbance due to an elevated abundance of oxygenic phototrophs would favor GSB over PSB (Brocks and Schaeffer, 2008). In any case, there appears to be a time lag of 50–100 years between the deposition of the most prominent flood layers (Fig 6c, marked with triangles) and the subsequent reorganizations of the sulfur bacteria community, so that it remains uncertain as to what exactly controlled past shifts in the microbial community structure in the Lake Cadagno water column.

A weakening of euxinic conditions as indicated by decreased Mo burial seems to be associated with an increase in flood frequency and the resulting episodic ventilation of the bottom waters. Indeed, enhanced flooding around 3.8, 3.4 and 2.5 kyr BP led to changes in the chemical and physical water properties and may also have influenced (directly or indirectly) the bacterial community. However, despite frequent flooding over decadal or even centennial periods, the chemocline quickly reestablished following such interruptive events.

6.2.2. Short-term oxidizing events indicated by peaks in S, Ca, Fe and Mn

In the XRF data, the overall flood-activity pattern is best reflected by variations in K abundance, while single

event deposits can be traced as concentration spikes of the elements S, Ca, Fe and, less pronounced ('smeared'), of Mn. In more detail, S, Ca and Fe show strong peaks associated with flood layers between 3 and 6 kyr BP, sometimes corresponding to distinctly thick deposits (see grey arrows in Fig. 6a), which are indicative for the short-term injection of large volumes of sediment-laden and O_2-rich waters penetrating the chemocline. This O_2 supply possibly enabled the episodic fixation of Fe and Ca in carbonate/sulfate minerals.

Mn shows a different behavior. Its concentration generally only increases at the top of, or above, massive mass-movement or flood deposits (Figs. 4 and 6a; white and black stars in 6a). We relate these peaks to 'short-term oxidizing events' due to the introduction of O_2-rich waters by underflows. Yet, Mn concentrations are distinctly lower and peaks are less sharp than in the intermediate, Mn-enriched period between 12.1 and 9.8 kyr BP. This can be explained with a rather poor preservation of the primary Mn signal in the sediments. If Mn layers formed during fast precipitation of Mn-(oxyhydr)oxides are not covered and trapped by clastic flood-derived material, these layers would become exposed to the reducing lake waters and therefore likely undergo reduction to Mn^{2+} (Crowe et al., 2008b). In any case, the fact that event layers are often associated with rather local peaks in S, Ca, Fe, and Mn confirms that these events reflect only short-term oxidizing events and no longer-term oxidation of the hypolimnetic waters.

6.3. Implications for the interpretation of Mn-rich layers in lacustrine and marine sediment records

The strong Mn enrichment in the early Holocene (~12.1 to 9.8 kyr BP) sediments of Lake Cadagno suggests that the injection of oxygenated water to the lake bottom over brief periods (i.e. a few days) favors the rapid formation and sedimentation of Mn-phases. Our study supports the hypothesis that rapid burial by clastic sediments is crucial for the preservation of high Mn enrichments in the sediments. This situation applies to Lake Cadagno only during the ~2300-year long redox transition period, when bottom waters were intermediately reducing and only intermittently sulfidic. In the future, studies using both detailed sedimentological information and Mn analysis on millimeter scales have a great potential to reveal Mn enrichments in other lacustrine and marine basins due to mixing of oxic and anoxic waters near the sediment surface. Depending on the environmental setting, such Mn enrichments may constitute a proxy for riverine input, wind stress or tsunami-induced waves on a time scale of hours to days, as well as for sea-/lake-level changes or bio-productivity on longer time scales.

6.4. Lake Cadagno Mo enrichment compared to marine euxinic systems

The persistently high sedimentary Mo concentration in Lake Cadagno (80–490 ppm) over the past 9800 years relative to catchment rocks (~0.5 ppm in gneiss and dolomite; Dahl et al., 2010a) is indeed impressive. Despite the fact that the Mo concentration in the riverine fluids (~8 nM) and subaquatic springs (>14 nM) are low compared to seawater (~105 nM) (Dahl et al., 2010a), the contents are of similar magnitude, or higher than, the highest values measured in marine systems, such as the Baltic Sea (191 ppm) and the Holocene portion of the Cariaco basin sediments (95 ppm) (Arnold et al., 2004; Neubert et al., 2008). It needs to be noted, however, that reported Mo concentrations are not sedimentation-rate corrected, rendering direct comparison between different studies difficult. Nevertheless, Mo enrichment in Lake Cadagno still seems exceptional, given that sedimentation rates of autochthonous organic material in Lace Cadagno are likely higher than in the above-mentioned marine basins. The reason for high sedimentary Mo enrichment in Lake Cadagno lies within the high water flux through the lake. This manifests in the relatively short residence time of water (~1–2 years) and Mo (~100 days) in the monimolimnion (Dahl et al., 2010a) relative to marine systems ($<10^3$ years; Algeo and Lyons, 2006). In addition, we suggest that comparatively high fluxes of sedimentary organic carbon from bacterial biosynthesis at the chemocline have contributed to enhanced Mo sequestration into the Lake Cadagno sediments (Dahl et al., 2010a; Helz et al., 2011). The observed Mo-TOC relation (Fig. 9) indicates that highly reactive Mo is quantitatively scavenged into the sediments by adsorption onto or complexation with sinking organic matter. The combination of a large Mo flux through the lake (despite low Mo concentrations in source fluids), permanently stratified and euxinic conditions in the deeper portions of the lake, and comparatively large fluxes of organic matter conduces to an efficient Mo extraction mechanism in Lake Cadagno.

7. CONCLUSIONS

We applied a novel interdisciplinary approach studying high-resolution XRF core scanning records of redox-sensitive metals (Mn and Mo), variations in the phototrophic sulfur bacteria population, as well as climate-induced changes in the sedimentary facies to characterize and interpret redox-state variations in the Lake Cadagno water column during the Holocene. Our results provide conclusive evidence for an early oxic-intermediate-sulfidic redox-transition period shortly after glacial retreat and lake formation at ~12.5 kyr BP. The ~2300-year long intermediate, Mn-enriched, period lasting from ~12.1 to 9.8 kyr BP is characterized by strongly fluctuating Mn concentrations in the sediments and first evidence for efficient Mo burial. Mn^{2+} is intensely leached from the sediments in contact with the reducing lake waters during this initial phase of sulfidic conditions with a still rather unstable, or not permanently stratified, water-column. Enhanced precipitation and trapping of Mn-(oxyhydr)oxides is associated with episodic water column mixing due to flood-induced underflows. In addition, the appearance of phototrophic sulfur bacteria populations with the onset of the Mn-enriched period confirms the beginning of weak/intermittent sulfidic conditions. At the end of this period with intermediate redox conditions 9800 ± 130 years ago, a pronounced drop of Mn and a simultaneous rise in Mo concentrations in the sediments

indicate efficient Mo burial in a sulfidic water column, and thus the onset of euxinic conditions in Lake Cadagno. We speculate that this redox transition was causally linked to the contemporaneous climate warming, which led to permafrost melting and the activation of the subaquatic springs. The inflow of salt-rich waters to the lake bottom likely initiated the formation of a stable chemocline and water-column stratification in the early Holocene. We found geochemical evidence that Lake Cadagno remained sulfidic throughout the Holocene until today. Flood and mass-movement events, however, generated turbiditic underflows that sporadically introduced O_2-rich water to the hypolimnion, thus temporarily weakening the sulfidic conditions. Frequent occurrence of such events may have lastingly affected water turbidity and nutrient supply, and may thus have caused shifts in the microbial community structure, from a PSB- to a GSB-dominated bacterial population.

Our study emphasizes the value and reliability of high-resolution XRF core scanning records of Mn and Mo for paleoenvironmental redox reconstructions. Whereas conventional elemental analysis may most often be lacking the necessary resolution to study laminated sediments with millimeter-scale lithologic variations, XRF scanning has the feasibility of representing these high-frequency chemical changes. We suggest that high-resolution Mn records from anoxic lacustrine and marine systems allow for the reconstruction of past short-term water-column mixing and/or ventilation events induced by changes in wind stress, riverine input (flood events), tsunami-induced waves (in coastal lakes), or lake/sea-level fluctuations. Therefore, our results highlight the great potential of XRF core scanning to obtain novel constraints on paleo-environmental reconstructions. On a more technical side, the calibration of XRF counts by quantitative elemental analyses (here ICP-MS) seems particularly important in the case of redox-sensitive elements, as only then comparison with other sedimentary records is possible. In addition, alteration of mineral phases at the sediment surface after core opening can bias scanning results. Furthermore, the here-applied approach is directly applicable to other aquatic environments with uncertain redox history, yet it hinges on the capacity to detect Mo. The application of XRF core scanning may thus be problematic in the case of very low (but still diagnostic) Mo concentrations.

For the Lake Cadagno sediments, however, the consistency between the bacterial DNA and (redox-indicating) carotenoid pigment records on the one hand, and the XRF record on the other hand validates our multi-proxy approach to reconstruct lacustrine redox conditions in the past. In conclusion, Lake Cadagno provides a unique natural facility to study geochemical redox processes, to calibrate paleoenvironmental proxies and to investigate the evolution of the phototrophic sulfur bacterial community during changing environmental conditions and climatic events over the past ~12,000 years.

ACKNOWLEDGEMENTS

We thank Matteo Bonalumi, Lukas Glur, Robert Hoffmann and Ulrike van Raden for their help in the field. We are also thankful to Marian Fujak who measured radionuclide activities. Hermann Mönch and Annette Johnson greatly assisted with ICP-MS measurements. We also like to thank the Alpine Biology Center Piora (CBA) for supporting this study and for the logistic assistance during fieldwork. Comments from Christian März, Jochen Brocks, and two anonymous reviewers largely improved this manuscript. This study is part of the project 'FloodAlp! Frequency and intensity of extreme floods in the Alps through the Holocene and implications for natural hazards in future climate scenarios' funded by the Swiss National Science Foundation (SNF) (Grant 200021-121909). The study also benefitted from an SNF R'Equip fund granted to M.F.L. T.W.D. thanks the Villum Foundation and the Danish National Research Foundation (NordCEE, DNRF53) for financial support.

REFERENCES

Algeo T. J. and Lyons T. W. (2006) Mo-total organic carbon covariation in modern anoxic marine environments: implications for analysis of paleoredox and paleohydrographic conditions. *Paleoceanography* **21**, PA1016. http://dx.doi.org/10.1029/2004PA001112.

Anbar A. D., Duan Y., Lyons T. W., Arnold G. L., Kendall B., Creaser R. A., Kaufman A. J., Gordon G. W., Scott C., Garvin J. and Buick R. (2007) A whiff of oxygen before the great oxidation event? *Science* **317**, 1903–1906.

Appleby P. G. (2001) Chronostratigraphic techniques in recent sediments. In *Tracking Environmental Change Using Lake Sediments, vol. 1: Basin Analysis, Coring, and Chronological Techniqes* (eds. W. M. Last and J. P. Smol). Kluwer Academic Publishers, Dordrecht, pp. 171–203.

Arnold G. L., Anbar A. D., Barling J. and Lyons T. W. (2004) Molybdenum isotope evidence for widespread anoxia in mid-proterozoic oceans. *Science* **304**, 87–90.

Bellanca A., Masetti D., Neri R. and Venezia F. (1999) Geochemical and sedimentological evidence of productivity cycles recorded in Toarcian black shales from the Belluno Basin, Southern Alps, northern Italy. *J. Sediment. Res.* **69**, 466–476.

Bernasconi S. M., Bauder A., Bourdon B., Brunner I., Bünemann E., Chris I., Derungs N., Edwards P., Farinotti D., Frey B., Frossard E., Furrer G., Gierga M., Göransson H., Gülland K., Hagedorn F., Hajdas I., Hindshaw R., Ivy-Ochs S., Jansa J., Jonas T., Kiczka M., Kretzschmar R., Lemarchand E., Luster J., Magnusson J., Mitchell E. A. D., Venterink H. O., Plötze M., Reynolds B., Smittenberg R. H., Stähli M., Tamburini F., Tipper E. T., Wacker L., Welc M., Wiederhold J. G., Zeyer J., Zimmermann S. and Zumsteg A. (2011) Chemical and biological gradients along the Damma glacier soil chronosequence, Switzerland. *Vadose Zone J.* **10**, 867–883.

Biebl H. and Pfennig N. (1978) Growth yields of green sulfur bacteria in mixed cultures with sulfur and sulfate reducing bacteria. *Arch. Microbiol.* **117**, 9–16.

Birch L., Hanselmann K. W. and Bachofen R. (1996) Heavy metal conservation in Lake Cadagno sediments: Historical records of anthropogenic emissions in a meromictic Alpine lake. *Water Res.* **30**, 679–687.

Blaauw M. (2010) Methods and code for 'classical' age-modelling of radiocarbon sequences. *Quat. Geochronol.* **5**, 512–518.

Bligh E. G. and Dyer W. J. (1959) A rapid method of total lipid extraction and purification. *Can. J. Biochem. Physiol.* **37**, 911–917.

Böning P., Bard E. and Rose J. (2007) Toward direct, micron-scale XRF elemental maps and quantitative profiles of wet marine sediments. *Geochem. Geophys. Geosyst.* **8**, Q05004. http://dx.doi.org/10.1029/2006GC001480.

Bostick B. C., Fendorf S. and Helz G. R. (2002) differential adsorption of molybdate and tetrathiomolybdate on pyrite (FeS_2). *Environ. Sci. Technol.* **37**, 285–291.

Brocks J. J., Love G. D., Summons R. E., Knoll A. H., Logan G. A. and Bowden S. A. (2005) Biomarker evidence for green and purple sulphur bacteria in a stratified Palaeoproterozoic sea. *Nature* **437**, 866–870.

Brocks J. J. and Schaeffer P. (2008) Okenane, a biomarker for purple sulfur bacteria (Chromatiaceae), and other new carotenoid derivatives from the 1640 Ma Barney Creek Formation. *Geochim. Cosmochim. Acta* **72**, 1396–1414.

Canfield D. E., Poulton S. W., Knoll A. H., Narbonne G. M., Ross G., Goldberg T. and Strauss H. (2008) Ferruginous conditions dominated later neoproterozoic deep-water chemistry. *Science* **321**, 949–952.

Canfield D. E. and Thamdrup B. (2009) Towards a consistent classification scheme for geochemical environments, or, why we wish the term 'suboxic' would go away. *Geobiology* **7**, 385–392.

Canfield D. E., Thamdrup B. and Hansen J. W. (1993) The anaerobic degradation of organic matter in Danish coastal sediments: iron reduction, manganese reduction, and sulfate reduction. *Geochim. Cosmochim. Acta* **57**, 3867–3883.

Calvert S. E. and Pedersen T. F. (1996) Sedimentary geochemistry of manganese: implications for the environment of formation of manganiferous black shales. *Econ. Geol.* **91**, 36–47.

Cartapanis O., Tachikawa K. and Bard E. (2011) Northeastern Pacific oxygen minimum zone variability over the past 70 kyr: Impact of biological production and oceanic ventilation. *Paleoceanography* **26**, PA4208. http://dx.doi.org/10.1029/2011PA002126.

Christie W. W. (1989) *Gas Chromatography and Lipids: A Practical Guide*. The Oily Press Ltd., 191 pp.

Crowe S. A., Jones C., Katsev S., Magen C., O'Neill A. H., Sturm A., Canfield D. E., Haffner G. D., Mucci A., Sundby B. and Fowle D. A. (2008a) Photoferrotrophs thrive in an Archean Ocean analogue. *Proc. Natl. Acad. Sci. USA* **105**, 15938–15943.

Crowe S. A., O'Neill A. H., Katsev S., Hehanussa P., Haffner G. D., Sundby B., Mucci A. and Fowle D. A. (2008b) The biogeochemistry of tropical lakes: a case study from Lake Matano, Indonesia. *Limnol. Oceanogr.* **53**, 319–331.

Crusius J., Calvert S., Pedersen T. and Sage D. (1996) Rhenium and molybdenum enrichments in sediments as indicators of oxic, suboxic and sulfidic conditions of deposition. *Earth Planet. Sci. Lett.* **145**, 65–78.

Dahl T. W., Anbar A. D., Gordon G. W., Rosing M. T., Frei R. and Canfield D. E. (2010a) The behavior of molybdenum and its isotopes across the chemocline and in the sediments of sulfidic Lake Cadagno, Switzerland. *Geochim. Cosmochim. Acta* **74**, 144–163.

Dahl T. W., Chappaz A., Fitts J. P. and Lyons T. W. (2013) Molybdenum reduction in a sulfidic lake: evidence from X-ray absorption fine-structure spectroscopy and implications for the Mo paleoproxy. *Geochim. Cosmochim. Acta* **103**, 213–231.

Dahl T. W., Hammarlund E. U., Anbar A. D., Bond D. P. G., Gill B. C., Gordon G. W., Knoll A. H., Nielsen A. T., Schovsbo N. H. and Canfield D. E. (2010b) Devonian rise in atmospheric oxygen correlated to the radiations of terrestrial plants and predatory fish. *Proc. Natl. Acad. Sci. USA* **107**, 17911–17915.

Davison W. (1993) Iron and manganese in lakes. *Earth Sci. Rev.* **34**, 119–163.

De Cesare G., Boillat J. and Schleiss A. (2006) Circulation in stratified lakes due to flood-induced turbidity currents. *J. Environ. Eng.* **132**, 1508–1517.

Decristophoris P. M. A., Peduzzi S., Ruggeri-Bernardi N., Hahn D. and Tonolla M. (2009) Fine scale analysis of shifts in bacterial community structure in the chemocline of meromictic Lake Cadagno, Switzerland. *J. Limnol.* **68**, 16–24.

Del Don C., Hanselmann K. W., Peduzzi R. and Bachofen R. (2001) The meromictic alpine Lake Cadagno: orographical and biogeochemical description. *Aquat. Sci.* **63**, 70–90.

Elvert M., Boetius A., Knittel K. and Jørgensen B. B. (2003) Characterization of specific membrane fatty acids as chemotaxonomic markers for sulfate-reducing bacteria involved in anaerobic oxidation of methane. *Geomicrobiol. J.* **20**, 403–419.

Emerson S. and Huested S. S. (1991) Ocean anoxia and the concentrations of molybdenum and vanadium in seawater. *Mar. Chem.* **34**, 177–196.

Erickson B. E. and Helz G. R. (2000) Molybdenum(VI) speciation in sulfidic waters: stability and lability of thiomolybdates. *Geochim. Cosmochim. Acta* **64**, 1149–1158.

Froelich P. N., Klinkhammer G. P., Bender M. L., Luedtke N. A., Heath G. R., Cullen D. and Dauphin P. (1979) Early oxidation of organic matter in pelagic sediments of the eastern equatorial Atlantic: suboxic diagenesis. *Geochim. Cosmochim. Acta* **43**, 1075–1090.

Giguet-Covex C., Arnaud F., Poulenard J., Disnar J.-R., Delhon C., Francus P., David F., Enters D., Rey P.-J. and Delannoy J.-J. (2011) Changes in erosion patterns during the Holocene in a currently treeless subalpine catchment inferred from lake sediment geochemistry (Lake Anterne, 2063 m a.s.l., NW French Alps): the role of climate and human activities. *The Holocene* **21**, 651–665.

Gilli A., Anselmetti F. S., Glur L. and Wirth S. B. (2013) Lake sediments as archives of recurrence rates and intensities of past flood events. In *Dating torrential processes on fans and cones – Methods and their application for hazard and risk assessment*, vol. 47 (eds. M. Schneuwly-Bollschweiler, M. Stoffel and F. Rudolf-Miklau). Advances in Global Change Research, Springer, USA, pp. 225–242, doi: 10.1007/978-94-007-4336-6_15.

Girardclos S., Schmidt O. T., Sturm M., Ariztegui D., Pugin A. and Anselmetti F. S. (2007) The 1996 AD delta collapse and large turbidite in Lake Brienz. *Mar. Geol.* **241**, 137–154.

Goldberg T., Archer C., Vance D., Thamdrup B., McAnena A. and Poulton S. W. (2012) Controls on Mo isotope fractionations in Mn-rich anoxic marine sediment, Gullmar Fjord, Sweden. *Chem. Geol.* **296–297**, 73–82.

Gregersen L. H., Habicht K. S., Peduzzi S., Tonolla M., Canfield D. E., Miller M., Cox R. P. and Frigaard N.-U. (2009) Dominance of a clonal green sulfur bacterial population in a stratified lake. *FEMS Microbiol. Ecol.* **70**, 30–41.

Grill E. V. (1982) Kinetic and thermodynamic factors controlling manganese concentrations in oceanic waters. *Geochim. Cosmochim. Acta* **46**, 2435–2446.

Habicht K. S., Miller M., Cox R. P., Frigaard N.-U., Tonolla M., Peduzzi S., Falkenby L. G. and Andersen J. S. (2011) Comparative proteomics and activity of a green sulfur bacterium through the water column of Lake Cadagno, Switzerland. *Environ. Microbiol.* **13**, 203–215.

Hebting Y., Schaeffer P., Behrens A., Adam P., Schmitt G., Schneckenburger P., Bernasconi S. M. and Albrecht P. (2006) Biomarker evidence for a major preservation pathway of sedimentary organic carbon. *Science* **312**, 1627–1631.

Helz G. R., Bura-Nakić E., Mikac N. and Ciglenečki I. (2011) New model for molybdenum behavior in euxinic waters. *Chem. Geol.* **284**, 323–332.

Helz G. R., Vorlicek T. P. and Kahn M. D. (2004) Molybdenum scavenging by iron monosulfide. *Environ. Sci. Technol.* **38**, 4263–4268.

Hennekam R. and de Lange G. (2012) X-ray fluorescence core scanning of wet marine sediments: methods to improve quality

and reproducibility of highresolution paleoenvironmental records. *Limnol. Oceanogr. Methods* **10**, 991–1003.

Huckriede H. and Meischner D. (1996) Origin and environment of manganese-rich sediments within black-shale basins. *Geochim. Cosmochim. Acta* **60**, 1399–1413.

Itoh N., Tani Y., Nagatani T. and Soma M. (2003) Phototrophic activity and redox condition in Lake Hamana, Japan, indicated by sedimentary photosynthetic pigments and molybdenum over the last 250 years. *J. Paleolimnol.* **29**, 403–422.

Jansen J. H. F., Van der Gaast S. J., Koster B. and Vaars A. J. (1998) CORTEX, a shipboard XRF-scanner for element analyses in split sediment cores. *Mar. Geol.* **151**, 143–153.

Jones C., Crowe S. A., Sturm A., Leslie K. L., MacLean L. C. W., Katsev S., Henny C., Fowle D. A. and Canfield D. E. (2011) Biogeochemistry of manganese in ferruginous Lake Matano, Indonesia. *Biogeosciences* **8**, 2977–2991.

Krige L. J. (1917) Petrographische Untersuchungen im Val Piora und Umgebung. *Eclogae Geol. Helv.* **14**, 519–654.

Learman D. R., Wankel S. D., Webb S. M., Martinez N., Madden A. S. and Hansel C. M. (2011) Coupled biotic–abiotic Mn(II) oxidation pathway mediates the formation and structural evolution of biogenic Mn oxides. *Geochim. Cosmochim. Acta* **75**, 6048–6063.

Löwemark L., Jakobsson M., Mörth M. and Backman J. (2008) Arctic Ocean manganese contents and sediment colour cycles. *Polar Res.* **27**, 105–113.

Lyons T. W., Anbar A. D., Severmann S., Scott C. and Gill B. C. (2009) Tracking euxinia in the ancient ocean: a multiproxy perspective and proterozoic case study. *Annu. Rev. Earth Planet. Sci.* **37**, 507–534.

Manske A. K., Glaeser J., Kuypers M. M. M. and Overmann J. (2005) Physiology and phylogeny of green sulfur bacteria forming a monospecific phototrophic assemblage at a depth of 100 meters in the Black Sea. *Appl. Environ. Microbiol.* **71**, 8049–8060.

März C., Stratmann A., Matthiessen J., Meinhardt A. K., Eckert S., Schnetger B., Vogt C., Stein R. and Brumsack H. J. (2011) Manganese-rich brown layers in Arctic Ocean sediments: composition, formation mechanisms, and diagenetic overprint. *Geochim. Cosmochim. Acta* **75**, 7668–7687.

Meyer K. M., Macalady J. L., Fulton J. M., Kump L. R., Schaperdoth I. and Freeman K. H. (2011) Carotenoid biomarkers as an imperfect reflection of the anoxygenic phototrophic community in meromictic Fayetteville Green Lake. *Geobiology* **9**, 321–329.

Middelburg J. J., de Lange G. J. and Van der Weijden C. H. (1987) Manganese solubility control in marine pore waters. *Geochim. Cosmochim. Acta* **51**, 759–763.

Morgan J. J. (2005) Kinetics of reaction between O_2 and Mn(II) species in aqueous solutions. *Geochim. Cosmochim. Acta* **69**, 35–48.

Mulder T. and Alexander J. (2001) The physical character of subaqueous sedimentary density flows and their deposits. *Sedimentology* **48**, 269–299.

Musat N., Halm H., Winterholler B., Hoppe P., Peduzzi S., Hillion F., Horreard F., Amann R., Jørgensen B. B. and Kuypers M. M. M. (2008) A single-cell view on the ecophysiology of anaerobic phototrophic bacteria. *Proc. Natl. Acad. Sci. PNAS* **105**, 17861–17866.

Nägler T. F., Neubert N., Böttther M. E., Dellwig O. and Schnetger B. (2011) Molybdenum isotope fractionation in pelagic euxinia: evidence from the modern Black and Baltic Seas. *Chem. Geol.* **289**, 1–11.

Nägler T. F., Siebert C., Lüschen H. and Böttcher M. E. (2005) Sedimentary Mo isotope records across the Holocene fresh-brackish water transition of the Black Sea. *Chem. Geol.* **219**, 283–295.

Neubert N., Nägler T. F. and Böttther M. E. (2008) Sulfidity controls molybdenum isotope fractionation into euxinic sediments: evidence from the modern Black Sea. *Geology* **36**, 775–778.

Niemann H., Stadnitskaia A., Wirth S. B., Gilli A., Anselmetti F. S., Sinninghe Damsté J. S., Schouten S., Hopmans E. C. and Lehmann M. F. (2012) Bacterial GDGTs in Holocene sediments and catchment soils of a high Alpine lake: application of the MBT/CBT-paleothermometer. *Clim. Past* **8**, 889–906. http://dx.doi.org/10.5194/cp-8-889-2012.

Peduzzi S., Storelli N., Welsh A., Peduzzi R., Hahn D., Perret X. and Tonolla M. (2012) *Candidatus* "Thiodictyon syntrophicum", sp. nov., a new purple sulfur bacterium isolated from the chemocline of Lake Cadagno forming aggregates and specific associations with *Desulfocapsa* sp.. *Syst. Appl. Microbiol.* **35**, 139–144.

Peduzzi S., Welsh A., Demarta A., Decristophoris P., Peduzzi R., Hahn D. and Tonolla M. (2011) Thiocystis chemoclinalis sp. nov. and Thiocystis cadagnonensis sp. nov., motile purple sulfur bacteria isolated from the chemocline of a meromictic lake. *Int. J. Syst. Evol. Microbiol.* **61**, 1682–1687.

Ravasi D. F., Peduzzi S., Guidi V., Peduzzi R., Wirth S. B., Gilli A. and Tonolla M. (2012) Development of a real-time PCR method for the detection of fossil 16S rDNA fragments of phototrophic sulfur bacteria in the sediments of Lake Cadagno. *Geobiology* **10**, 196–204. http://dx.doi.org/10.1111/j.1472-4669.2012.00326.x.

Reimer P. J., Baillie M. G. L., Bard E., Bayliss A., Beck J. W., Blackwell P. G., Bronk Ramsey C., Buck C. E., Burr G. S., Edwards R. L., Friedrich M., Grootes P. M., Guilderson T. P., Hajdas I., Heaton T. J., Hogg A. G., Hughen K. A., Kaiser K. F., Kromer B., McCormac F. G., Manning S. W., Reimer R. W., Richards D. A., Southon J. R., Talamo S., Turney C. S. M., van der Plicht J. and Weyhenmeyer C. E. (2009) IntCal09 and Marine09 Radiocarbon Age calibration curves, 0–50,000 years cal BP. *Radiocarbon* **51**, 1111–1150.

Richter T. O., van der Gaast S., Koster B., Vaars A., Gieles R., de Stigter H. C., de Haas H. and van Weering T. C. E. (2006) The Avaatech XRF Core Scanner: technical description and applications to NE Atlantic sediments. In *New Techniques in Sediment Core Analysis*, vol. 267 (ed. R. G. Rothwell). Geological Society, London, Special Publications, pp. 39–50.

Sabatino N., Neri R., Bellanca A., Jenkyns H. C., Masetti D. and Scopelliti G. (2011) Petrography and high-resolution geochemical records of Lower Jurassic manganese-rich deposits from Monte Mangart, Julian Alps. *Palaeogeogr. Palaeoclimatol. Palaeoecol.* **299**, 97–109.

Schaller T. and Wehrli B. (1997) Geochemical-focusing of manganese in lake sediments – an indicator of deep-water oxygen conditions. *Aquat. Geochem.* **2**, 359–378.

Schnellmann M. S., Anselmetti F. S., Giradini D., McKenzie J. A. and Ward S. N. (2002) Prehistoric earthquake history revealed by lacustrine slump deposits. *Geology* **30**, 1131–1134.

Scott C. and Lyons T. W. (2012) Contrasting molybdenum cycling and isotopic properties in euxinic versus non-euxinic sediments and sedimentary rocks: refining the paleoproxies. *Chem. Geol.*. http://dx.doi.org/10.1016/j.chemgeo.2012.05.012.

Spofforth D. J. A., Pälike H. and Green D. (2008) Paleogene record of elemental concentrations in sediments from the Arctic Ocean obtained by XRF analyses. *Paleoceanography* **23**, PA1S09. http://dx.doi.org/10.1029/2007PA001489.

Thevenon F., Adatte T., Spangenberg J. E. and Anselmetti F. S. (2012) Elemental (C/N ratios) and isotopic (δ^{15}Norg, δ^{13}Corg)

compositions of sedimentary organic matter from a high-altitude mountain lake (Meidsee, 2661 m a.s.l., Switzerland): implications for Lateglacial and Holocene Alpine landscape evolution. *The Holocene* **22**, 1135–1142.

Tjallingii R., Röhl U., Kölling M. and Bickert T. (2007) Influence of the water content on X-ray fluorescence corescanning measurements in soft marine sediments. *Geochem. Geophys. Geosyst.* **8**, Q02004. http://dx.doi.org/10.1029/2006GC001393.

Tonolla M., Peduzzi S., Demarta A., Peduzzi R. and Hahn D. (2004) Phototropic sulfur and sulfate-reducing bacteria in the chemocline of meromictic Lake Cadagno, Switzerland. *J. Limnol.* **63**, 161–170.

Tonolla M., Peduzzi R. and Hahn D. (2005) Long-term population dynamics of phototrophic sulfur bacteria in the chemocline of Lake Cadagno, Switzerland. *Appl. Environ. Microbiol.* **71**, 3544–3550. http://dx.doi.org/10.1128/AEM.71.7.3544-3550.2005.

Vorlicek T. P., Kahn M. D., Kasuya Y. and Helz G. R. (2004) Capture of molybdenum in pyrite-forming sediments: role of ligand-induced reduction by polysulfides. *Geochim. Cosmochim. Acta* **68**, 547–556.

Wirth S. B., Girardclos S., Rellstab C. and Anselmetti F. S. (2011) The sedimentary response to a pioneer geo-engineering project: tracking the Kander River deviation in the sediments of Lake Thun (Switzerland). *Sedimentology* **58**, 1737–1761.

Ziegler M., Jilbert T., de Lange G. J., Lourens L. J. and Reichart G.-J. (2008) Bromine counts from XRF scanning as an estimate of the marine organic carbon content of sediment cores. *Geochem. Geophys. Geosyst.* **9**. http://dx.doi.org/10.1029/2007GC001932.

Associate editor: Jochen J. Brocks